The Pennsylvania State University

The Graduate School

Intercollege Graduate Program in Materials

CRITICAL ISSUES OF COMPLEX, EPITAXIAL OXIDE GROWTH AND

INTEGRATION WITH SILICON BY MOLECULAR BEAM EPITAXY

A Thesis in

Materials

by

James Lettieri

Submitted in Partial Fulfillment

of the Requirements

for the Degree of

Doctor of Philosophy

December 2002

We approve the thesis of James Lettieri.

Date of Signature

_____   _____

Darrell G. Schlom
Professor of Materials Science and Engineering
Thesis Advisor
Chair of Committee

_____   _____

Venkatraman Gopalan
Assistant Professor of Materials Science and Engineering

_____   _____

Xiaoxing Xi
Associate Professor of Physics and Materials Science
and Engineering

_____   _____

Thomas E. Mallouk
Dupont Professor of Materials Chemistry

_____   _____

Barbara A. Shaw
Associate Professor of Engineering Science and Mechanics
Chair of the Intercollege Program in Materials

Abstract

Molecular beam epitaxy was used to grow epitaxial oxides on silicon substrates using a systematic approach beginning with an understanding of system oxidation kinetics and thermodynamics and involving a strategy of moving from simple binary oxides to more complex structures. The growth of BaO, SrO, EuO, and SrTiO$_3$ are discussed with a focus on the general theme of integration of functional, epitaxial oxides into a silicon environment.

Oxidation studies of various metal systems relevant for oxide on silicon epitaxy and integration are reported. Experimental results demonstrate dramatically different oxidation behavior depending on elemental species and the catalytic nature of an alkaline earth metal at small doping concentrations to enable the full oxidation of the poorly oxidizing metals at oxygen pressures significantly lower than during deposition of the pure metal alone. Results from the deposition of Sr, Ba, Ti, La, Eu, Gd, and Al and codeposited combinations of the various elements are presented.

The critical aspects of the growth of alkaline earth oxides on silicon are explained in detail. The step by step transition from the silicon to the alkaline earth oxide mediated by the formation of an interfacial silicide layer as described through reflection high energy electron diffraction (RHEED) is presented and used as a means to understand issues related to interface stability, oxidation, structural, and strain considerations for each stage of the growth. High quality, commensurate alkaline earth oxides (BaO, SrO, and (Ba,Sr)O) are grown on silicon at room temperature and $P_{O2\ background} \sim 3 \times 10^{-8}$ Torr,

taking advantage of the favorable oxidation kinetics of the alkaline earth metals and anomalously low temperatures necessary for epitaxial growth.

The growth of alkaline earth oxide and rare earth earth oxide solid solutions and rare earth oxides (EuO) are described. RHEED data demonstrates the ability to create metastable solid solutions. The first reported epitaxial EuO (a silicon compatible ferromagnet) on silicon is reported, enabled by the use of a thin buffer layer (13 Å) of SrO. X-ray diffraction and RHEED data indicate single phase, single domain films with tremendous potential for spintronics applications.

Using a strategy of transition from simple structures to the more complex, the growth of a perovskite ($SrTiO_3$) on silicon is demonstated. Growth of a structurally optimized perovskite structure entails the transformation of a thin interfacial alkaline earth oxide layer into the initial perovskite cells. Such a transformation is facilitated by the strong tendency of the system to form the equilibrium structure under silicon friendly growth conditions (low temperature and low oxidant pressure). Optimized $SrTiO_3$ and La-doped $SrTiO_3$ on silicon are used to integrate a piezoelectric relevant for microelectromechanical systems (MEMS) applications and a ferroelectric relevant for a ferroelectric random access memory (FRAM) architecture. A d_{33} (piezoelectric coefficient) value of over 400 pm/V under bias is measured for the piezoelectric ($Pb(Mn_{1/3}Nb_{2/3})O_3 - PbTiO_3$) and a remanent polarization of 25 $\mu C/cm^2$ and fatigue free behavior ($>10^{12}$ cycles) for a low temperature (450 °C) deposited ferroelectric ($Pb(Zr,Ti)O_3$) is obtained.

Initial work concerning the growth of even more complex structures such as conducting and ferroelectric superlattices are described. Short period superlattices of

LaTiO$_3$ and SrTiO$_3$ are successfully grown on silicon with a high degree of crystalline quality. Future directions for more complex oxide integration and nonoxide integration are proposed.

1.0 Introduction and Statement of Goals

1.1 Introduction

The successful synergy of disparate materials often presents a difficult challenge to the scientist while simultaneously providing the prospect of virtually limitless potential. Whether in a macrocopic mechanical sense, as with a gear in a network of complex machinery, a microscopic sense, as with an integrated circuit comprised of millions of electronic components, or an atoscopic sense, as with manipulation of an electron in a single molecule through a field effect, the union of dissimilar materials offers the promise of a cooperative unit representing a whole that is more fruitful than the sum of its parts. The critical difficulty lies with bringing these materials together in a mutually beneficial existence.

In the arena of thin film growth (the focus of this thesis), heteroepitaxy (the regularly oriented growth of one crystalline substance on another crystalline substance) offers a means to achieve this end. Heteroepitaxial growth allows one to bring multiple materials together in a very controlled manner, where a truly cooperative structure can function at its highest potential. The heteroepitaxial growth of oxides on semiconductors, and specifically silicon, for example, presents significant opportunities to harness the versatile superconducting, dielectric, magnetic, non-linear optical, pyroelectric, piezoelectric, and ferroelectric properties of oxides while simultaneously exploiting the properties of the underlying semiconductor. To create epitaxial structures in which the properties of the strongly differing underlying silicon and overlying oxide film both attain

their full potential, control of the silicon/oxide interface is critical. Heteroepitxaial growth on silicon, however, presents serious complications concerning reactivity between the desired oxide and silicon and delicate oxidation considerations. Only through understanding these concerns and difficulties can the successful union of these materials be achieved.

The recent success of various groups pursuing oxide on silicon heteroepitaxy for application in novel transistor structures represents a key achievement in the field.[1,2] Although a number of critical difficulties and impediments concerning the ultimate viability of these heterostructures in an industrial setting exist these results strongly demonstrate a proof of concept and offer a promise of future, unparalleled utility. The complete and ultimate realization of this utility will be predicated on four key factors: (1) a total understanding of the nature of the interface in relation to thermodynamic and kinetic issues, (2) the transfer of fundamental understanding into practical growth strategies, (3) the adaptation of these strategies to multiple material systems, and (4) the adaptation of new materials into new devices and heterostructures to fully exploit these new materials and their new functionalities. This thesis attempts to address these four key issues.

1.2 Statement of Goals

The goals of this thesis are classified as follows:

1. The investigation of the fundamental issues related to oxidation of metallic elements relevant for silicon integration. Oxidation represents one of the most basic parameters of any oxide film growth and plays an especially important role when growing on a highly reactive silicon substrate. Based on previous experience with the growth of complex oxides, oxidation has been a critical factor determining success or failure in many heteroepitaxial systems.

2. Development of the basic issues related to system thermodynamics, oxidation kinetics, previous growth approaches and knowledge of interfacial structures, and ultrahigh vacuum deposition concerns into novel strategies to grow alkaline earth oxides, rare earth oxides, and simple perovskite structures on silicon using molecular beam epitaxy. A successful strategy will address many of the concerns pertinent to the integration of these materials into working device structures.

3. Adaptation of novel growth strategies to novel material systems with the intent of introducing new functionalities into a silicon environment. Specifically, the growth of the previously unrealized epitaxial EuO on silicon will be explored with the intent of integrating a versatile oxide ferromagnetic material with a semiconductor. In a more general sense, the integration of both conductive alkaline earth oxides and conductive perovskites will be investigated.

4. Exploration of new heteroepitaxial oxide on silicon systems in existing and novel device structures designed to exploit the oxide functionality. Attention will be paid to the issues of integration of ferroelectric and piezoelectric materials and the use of $SrTiO_3$ as a platform for the growth of more complex (including nonoxide) structures on a silicon substrate. Prospects and potential for a number of material systems will be addressed.

---

1. R. A. McKee, F. J. Walker, and M. F. Chisholm, Science **293**, 468 (2001).

2. K. Eisenbeiser, J. M. Finder, Z. Yu, J. Ramdani, J. A. Curless, J. A. Hallmark, R. Droopad, W. J. Ooms, L. Salem, S. Bradshaw, and C. D. Overgaard, Appl. Phys. Lett. **76**, 1324 (2000).

2.0 Background

2.1 Historical Perspective

Although the science of epitaxial oxides on semiconductors has seen a recently renewed interest, the history of such heterostructures dates back nearly 70 years. In 1935, Yamaguti investigated the oxidation of single crystals of ZnS and the subsequent formation of ZnO by 'cathode ray reflection.'[1] While the techniques were understandably more rudimentary than techniques used presently and the concept of the integrated circuit was still many years in the future, one cannot help but notice a striking similarity between this work and work completed today. In fact, the basic ideas are quite similar, i.e., investigating a crystalline oxide/semiconductor interface with a surface sensitive diffraction technique.

A second, preliminary step was taken in 1951 by Sato using similar techniques to look at the growth of $ZnFe_2O_4$ on ZnS.[2] Even though $ZnFe_2O_4$ was not the expected result, it was identified correctly using electron diffraction. Sato postulated that the formation of the iron containing phase may have been due to the presence of impurities in the starting ZnS crystal. The results presented in this paper establish and highlight the same concerns important for crystalline oxide on silicon growth today, i.e. the concept of understanding reaction products, diffusion issues, and phase identification through electron diffraction.

The investigation of epitaxial oxides on semiconductors entered the modern era after the development of the integrated circuit in 1958. Indeed, the science of thin film

growth spurred by the invention of the transitor had a strong and positive impact on the growth and study of the oxide/semiconductor (and more specifically silicon) interface. The first example of the growth of an epitaxial oxide on silicon occurred in 1982 when Ihara *et al*. investigated the growth of $MgAl_2O_4$ on silicon using a vapor phase transport technique.[3] While the growth of a semiconductor on an oxide had been previously demonstrated (silicon on sapphire and spinel), Ihara *et al*. were the first to investigate the growth of spinel on silicon and the growth of silicon/spinel/silicon heterostructures. Although this work represented an important step in the use of a crystalline oxide in a silicon environment, the oxide was largely envisaged as a relatively passive component, acting as a dielectric insulator for electrical isolation.

Matsubara *et al*. made further progress with the growth of the first epitaxial perovskite on silicon through the use of a spinel buffer layer.[4] This work represented a key step, as it was the first demonstration of the growth of an epitaxial, perovskite oxide with the ultimate intent of utilizing an active functionality (e.g., piezoelectricity, ferroelectricity, etc.) found in perovskite materials. Although the concept had been proposed soon after the invention of the transistor, demonstration of such a growth would not be accomplished for a number of years.

The starting point for the research presented in this thesis, however, is traced to work completed by McKee *et al.* where they investigated the growth of $BaTiO_3/BaO/BaSi_2/Si$ heterostructures.[5] This work was neither the first epitaxial perovskite[4] nor the first epitaxial alkaline earth oxide[6] growth on silicon, however it was the first to propose the use of a stable silicide structure to enable the transition from the silicon to the oxide (which is the general concept used to grow the structures studied in

6

this thesis work). Additionally, it was the first result to truly demonstrate the formation

of an epitaxial oxide on silicon without the formation of an interfacial, amorphous SiO_2

layer.[7,8] Given the motivation for the growth of alternative gate dielectrics (instead of

the commonly used amorphous SiO_2) and the need to obtain high quality oxide/silicon

interfaces for MOSFET devices born in the late 1990s, this work represents a critical

result towards these ends. Along with the work by Matsubara *et al.* it was one of the first

studies to attempt to exploit the functionality of a complex oxide in a silicon

environment. This serves as the underlying idea behind the work presented here, with the

focus on not only understanding the fundamentals of oxide on semiconductor growth, but

also exploiting new oxides and new functionalities as well.

2.2 General Background on Experimental Techniques

Molecular beam epitaxy, reflection high energy electron diffraction, and four

circle x-ray diffraction served as the primary growth and characterization tools used in

this thesis. The following sections provide a brief overview and description of these

techniques.

2.2.1 Molecular Beam Epitaxy

Molecular beam epitaxy (MBE)[9] is a thin film physical vapor deposition

technique with demonstrated versatility and flexibility used to grow numerous complex

compounds. In MBE, films are grown through reactions that occur at a substrate surface

maintained in ultrahigh vacuum (UHV) conditions, where individual atomic species are delivered to the substrate in the form of thermally generated molecular beams. Maintenance of a molecular beam during deposition requires a low pressure growth environment to avoid scattering processes. While this dictates that growth rates are relatively slow (typically less than 1 monolayer (ML) / 5s) the control is unparalleled compared to other deposition techniques. The use and utility of *in situ* diagnostic tools during growth enabled by the controlled deposition conditions and UHV environment make MBE an extremely attractive tool for investigation of phenomena related to interface and growth science. Although a number of different techniques and diagnostic tools have been employed, the most well studied and perhaps the most useful is reflection high energy electron diffraction (RHEED). A detailed description of the RHEED characterization technique is provided in the next section.

MBE as a viable deposition process first drew significant interest in the late 1960s and early 1970s as a tool to examine the growth of III-V compound semiconductors. While the potential of III-V materials for electronic and optoelectronic devices is limitless, controlled synthesis is complicated by strongly differing vapor pressures of the constituent elements. The separate controls of the individual atomic species as well as the substrate temperature itself made MBE an attractive choice to explore the growth of these compounds.

Based on earlier fundamental studies examining delivery of atomic species, surface reaction processes, and the fundamentals of III-V growth,[10-13] significant progress was made in the 1980s with MBE. One of the most important advances and perhaps the most relevant to the work completed in this thesis concerned the progress made with the

8

understanding of RHEED as an *in situ* diagnostic tool to investigate surface structures[14,15] and growth evolution as studied through RHEED oscillations.[16-18] The understanding of these techniques has led to the growth of complex superlattice structures and interfacial engineering at the monolayer level and has been critical in the design and science of electronics that operate on the quantum scale.

Although much of the fundamental work with MBE was accomplished with III-V semiconductors, many of these results have been extended to other materials systems including II-VI semiconductors,[19,20] group IV semiconductors,[21] metal systems,[22] as well as most recently, oxides.[23] MBE growth of oxides serves as the focus of this thesis.

2.2.2 RHEED

RHEED[24,25] is a surface sensitive diffraction technique that is characterized by its nonintrusive nature during crystal growth and its surface sensitivity. In a RHEED geometry electrons are incident and forward scattered at a grazing angle of ~ 0.5-3.0°. Electrons generated by an electron gun used for RHEED analysis are typically 10-30 keV with low divergence, and are usually detected as a reciprocal space diffraction pattern on a phosphor screen. In many cases (as is the case with the instrument used in this thesis), a CCD camera is attached to the phosphor screen and interfaced with a computer for qualitative and quantitative analysis with standard RHEED software.

The unique geometry of the RHEED technique makes it especially useful for implementation on an MBE system. Indeed, the two techniques complement each other quite well. MBE offers atomic scale deposition precision in a UHV environment and

RHEED offers atomic scale information via an electron beam which can only function in a low pressure ambient. Although the geometry is optimal from a practical viewpoint, grazing incidence and the dynamical nature of the diffraction can often make analysis difficult.

Given the nature of the geometry and the energy of the impinging beam, RHEED is sensitive to the sample surface to a depth of a few monolayers. As a result, constraints are placed on the diffraction condition and the reciprocal space lattice devolves to a two-dimensional (2D) condition where diffraction is occurring from a 2D plane. Points in reciprocal space become infinite relrods perpendicular to the surface of the substrate because of this 2D geometrical constraint. The condition for diffraction becomes the intersection of the Ewald sphere and the reciprocal space lattice rods. Since the rods are infinite, every rod contributes to the diffraction event and the resulting pattern (for an ideal crystal) is a set of spots on a set of concentric rings (Laue circles). With a typical RHEED geometry usually half on the pattern is visible with the attention on the zeroth-order Laue circle. Particular focus is paid to the intersection of the (00) rod with the zeroth-ordered circle, which is termed the specular reflection. Monitoring the specular reflection as well as the position, shape, and intensity of the diffraction spots provides information concerning interfacial and surface structures, strain and relaxation processes, growth modes, and surface roughness. Details concerning each of these phenomena as interpreted through RHEED diffraction images and oscillations of the specular intensity during the growth of the oxides studied in this thesis are provided in detail in the following sections.

2.2.3 Four Circle X-ray Diffraction

Four circle x-ray diffraction[26] is an extremely useful technique for examining the

structural characteristics of epitaxial thin films or films with a high degree of orientation.

In addition to the standard two circles (θ or ω and 2θ) found in a typical powder

diffraction apparatus, the four circle tool has two additional degrees of freedom

represented by the angular designations ϕ and χ. (ω is defined as $\theta - 2\theta/2$). Figure 2.1

shows a schematic of the four circle geometry. While the ω and 2θ circles enable

probing of the crystalline planes in a film parallel to the surface of the substrate, the ϕ and

χ circles allow probing of reflections and planes that are not parallel to the substrate

surface. Unlike a randomly oriented powder or a randomly oriented film, an epitaxial

film displays a much lower symmetry where sets of diffraction planes occupy unique

positions in geometric space. Probing these reflections provides a wealth of information

not apparent through studying planes probed in a θ-2θ diffraction scan alone.

Three types of scans were performed during the course of this thesis: a θ-2θ scan,

an ω scan, and a ϕ scan. A θ-2θ scan (run at $\chi = 90°$ and termed an "on-axis scan") is a

scan where the ω and 2θ circles are moved simultaneously through angular space. As

with any other diffraction process, when the Bragg condition is satisfied, diffraction

events occur. Noting the specific angles at which this Bragg condition is satisfied

provides information concerning the interatomic spacing of the planes parallel to the

surface of the substrate. Peak position, peak shape, and peak width provides quantitative

information concerning the out-of-plane lattice constant, film strain (coherency or

11

incoherency), out-of-plane disorder along the film and substrate normal direction, film thickness, phase purity, and out-of plane crystallographic orientation.

The second type of scan employed in this thesis, termed an ω-scan, is one where the sample is moved to the angular position to satisfy the Bragg condition for a specific reflection and the sample is swept through ω angular space while the detector (2θ) is kept fixed. This type of scan (also conducted in an on-axis geometry) provides information concerning the miscut of a substrate (i.e., the angular difference between the physical surface normal and the normal of the crystallographic planes) as well as the spread and tilt of the film with respect to the substrate surface normal.

The third type of scan employed in this thesis, termed a ϕ-scan, is one where the sample is moved to the angular position to satisfy the Bragg condition for a specific reflection and a set of planes not parallel to the surface of the substrate (at an "off-axis position" or where χ no long is equal to 90°) is swept through ϕ angular space while all other angles are kept fixed. This scan reveals information about in-plane alignment, quantitative data concerning the in-plane mosaic spread of the film, and the symmetry of a given set of reflections.

2.3 Criteria for Epitaxial Oxide Growth on Silicon

Although virtually limitless in terms of potential complex metal oxide / silicon combinations, success in the epitaxial growth of these compounds relies heavily on an understanding of the fundamental constraints and criteria that govern the growth of these materials. The next two sections address these concerns, with the emphasis on what

materials one could potentially have success growing on silicon based on a thermodynamic analysis (Section 2.3.1) and the practical and physical implications with focus on the strategies one might broach to accomplish this growth (Section 2.3.2).

2.3.1 Thermodynamic Stability

Chemical reactivity plays a crucial role when examining heteroepitaxy in complex systems. To achieve high quality epitaxy, one needs to maintain a stable interface between the metal oxide and the silicon, and the loss of this interface through chemical reaction and the formation of interfacial phases (in this case silicates or amorphous silica and metal) will in a worst case, eliminate epitaxy. Although the consideration of chemical reactivity and thermodynamic stability is a critical concern for the growth of any thin film, this concern is magnified further when examining materials that are known to be extremely reactive (such as silicon) and in the most restrictive case of thin film growth, epitaxy.

Through consideration of thermodynamic stability along with other basic guidelines (i.e., solid and not radioactive), the choices for binary metal oxide on silicon epitaxy become severely restricted.[27,28] Indeed, the bulk of these materials fall into two classes of oxides, alkaline earth oxides and rare earth oxides. These thermodynamic calculations lead to a critical implication; alkaline earth oxides and rare earth oxides become a logical starting point for epitaxially integrating oxides with silicon. On a related note, one could imagine epitaxially integrating silicon-incompatible metal oxides if an intermediate layer of a stable compound (an alkaline earth oxide or rare earth oxide)

13

is grown first. These two ideas serve as the focus of this thesis, with the fundamental

approach to the growth of any complex oxide being step-wise in nature, beginning with

the growth of a simple, silicon compatible interfacial oxide and then transitioning to more

complex and possibly silicon incompatible structures. Given these limitations and this

approach, the growth of alkaline earth oxides and rare earth oxides serve as a starting

point for all the structures grown in this work (Chapters 5 and 6) and eventually lead to

the growth of more complex oxides and heterostructures (Chapters 7, 8, and 9).

2.3.2 Strategies for Epitaxial Growth

Since the formation of SiO_2 (especially at the earliest stages of the growth) can

have a strongly limiting effect on the quality of the subsequent epitaxial oxide growth,

one needs to be concerned with the overall oxygen pressure in the system. Three

strategies have been used to grow epitaxial oxides on silicon. The ultimate goal of all

three methods is to avoid the formation of an amorphous SiO_2 layer that would result in

the loss of the substrate's crystalline template before the oxide has a chance to nucleate

on it. The first strategy is to grow with no excess oxidant.[29-32] This could be achieved, for

example, through the use of a single reactant species having a stoichiometric

composition, e.g., by the supply of BaO molecules to the substrate surface. As most

oxides do not evaporate congruently, the supply of stoichiometric molecules of the

desired oxide to the substrate is a rare case unless non-equilibrium evaporation

techniques or specialized chemical precursors are used. Nonetheless, it has been used

recently to grow Y_2O_3,[29,30] CeO_2,[31] Pr_2O_3,[32] and Gd_2O_3[29,30] epitaxial films on silicon. An

14

easier method to deposit films is to use an excess oxidant environment, and the remaining two methods involve oxidant-rich growth conditions. The excess oxidant flux helps ensure that the deposited film will be fully oxidized. To prevent oxidation of the silicon substrate during the critical nucleation stage, two regimes of substrate temperature have been demonstrated for excess oxygen growth conditions: (1) high temperature, where SiO has sufficient volatility to keep the silicon surface free of SiO_2 for a low flux of oxidant and (2) low temperature, where the oxidation of silicon by the oxidant is sluggish due to kinetics. Most reports of the epitaxial growth of oxides on silicon fall into the high temperature / excess oxygen regime.[33-68] Although successful for the nucleation of an epitaxial oxide layer, these growth conditions typically lead to the growth of a SiO_2 layer at the silicon interface as the film thickens (and SiO can no longer make its way to the film surface to evaporate) due to the oxygen-rich growth conditions and high diffusivity of oxygen at high growth temperatures. When a SiO_2-free interface is required, either the first or the last of these three methods is desired. As the first can rarely be satisfied, the last of the three methods, the low temperature / excess oxygen regime is appealing.[5,8,69] It is in this low temperature / excess oxidant regime that assessing kinetic barriers to oxidation of the species being supplied to the substrate is critical. Issues concerning the oxidation kinetics of different species are addressed in Chapter 4. This thesis focuses on growth in the third regime.

2.4 General Background on Crystal Structures

Although many of the concerns investigated are applicable to the growth of any epitaxial oxide on silicon, this thesis focuses primarily on the growth of two specific oxide structures which are especially well suited to epitaxial growth on silicon: (1) the rock salt structure and (2) perovskite structure.

2.4.1 Rock Salt Structure

The rock salt structure shown schematically in Fig. 2.2 is one of the simplest binary metal oxide systems. The example shown in Fig. 2.2, SrO (one of the compounds grown in this study) exhibits the prototypical rock salt structure with space group Fm3m. The unit cell of this structure can be considered as an arrangement of two interpenetrating face-centered sublattices comprised of the anions and cations. In terms of coordination polyhedra, the anion and cation are at the centers of regular octahedra of the opposite species with an edge-sharing relationship. The cation coordination number is six. The alkaline earth oxides (BaO and SrO) and EuO exhibit this crystal structure.

2.4.2 Perovskite Structure

The perovskite structure is shown schematically in Fig. 2.3. The example shown in Fig. 2.3, $SrTiO_3$, exhibits the prototypical perovskite structure with space group Pm3m. The general formula for an oxide perovskite is ABO_3 with the A site cation in a 12-fold coordination and the B site cation in a 6-fold coordination. In a coordination polyhedra representation, the structure can also be considered as the A site cation sitting

at the center of a cube comprised of B-O octahedra. The perovskite structure is extremely accommodating and A and B can exist with 2+, 4+ ($SrTiO_3$), 3+, 3+ ($LaAlO_3$), 1+, 5+ ($NaNbO_3$), and 0, 6+ (ReO_3) valence combinations. Various other substitutions allowed by charge balance can also take place, including mixed substitutions which can form with ordered or disordered site occupancy.

Many of the pervoskites in this work show small distortions from the prototypical cubic cell that result in tetragonal (e.g., $BaTiO_3$, $Pb(Zr,Ti)O_3$) or orthorhombic ($SrRuO_3$) crystal structures. These distortions, which lower the crystal symmetry, often lead to interesting properties. For example, these distortions can lead to the tendency of the metal ions at the centers of the B-O octahedra to shift with respect to the lattice, causing dipoles and potentially ferroelectric compounds. As stated previously, perovskites exhibit a wide range of functionality, some of which are explored in this work.

Although the cubic perovskite prototype is three dimensional in nature, this structure can also be considered as a layered compound comprised of alternating "rock-salt like" sheets. This layered nature makes these compounds especially well suited for growth by MBE. Additionally, noting this similarity of structures between the rock salt and perovskite structure provides some insight for the strategies developed and explained in Chapter 7.

1. T. Yamaguti, Proc. Phys. Math. Soc. Jpn. **17**, 443 (1935).

2. R. Sato, J. Phys. Soc. Jpn. **6**, 527 (1951).

3. M. Ihara, Y. Arimoto, M. Jifuku, T. Kimura, S. Kodama, H. Yamawaki, and T. Yamaoka, J. Electrochem. Soc. **129**, 2569 (1982).

4. S. Matsubara, Jpn. J. Appl. Phys. **24** Suppl. 24-2, 10 (1985).

5. R.A. McKee, F.J. Walker, J.R. Conner, E.D. Specht, and D.E. Zelmon, Appl. Phys. Lett. **59**, 782 (1991).

6. Y. Kado and Y. Arita, Extended Abstracts of the 20th International Conference on Solid State Devices and Materials, Tokyo, 181 (1988).

7. Although the RHEED images shown by McKee *et al*. are insufficient to demonstrate the lack of SiO_2 at the oxide / silicon interface, corroborative work by McKee *et al*. in Ref. 8 was eventually published to support the original claim nearly eight years later.

8. R. A. McKee, F. J. Walker, and M. F. Chisholm, Phys. Rev. Lett. **81**, 3014 (1998)

9. *Molecular Beam Epitaxy – Fundamentals and Current Status* (Springer-Verlag, Berlin 1989) by M. A. Herman and H. Sitter is a good introductory text on both MBE theory and applications of the technique. Another highly recommended source is *Molecular Beam Epitaxy* (American Institute of Physics, New York 1994) edited by A. Y. Cho which provides a comprehensive compilation of the key papers and seminal work in the field of MBE growth through the early 1990s.

10. J. R. Arthur, J. Appl. Phys. **39**, 4032 (1968).

11. A. Y. Cho, Surf. Sci. **17**, 494 (1969).

12. A. Y. Cho, M. B. Panish, and I. Hayashi, Proc. Symp. GaAs and Related Compounds **2**, 18 (1970).

13. L. L. Chang, L. Esaki, W. E. Howard, and R. Ludeke, J. Vac. Sci. Technol. **10**, 11 (1973).

14. A. Y. Cho, J. Appl. Phys. **41**, 2780 (1970).

15. J. H. Neave and B. A. Joyce, J. Crystal Growth **44**, 387 (1978).

16. J. J. Harris, B. A. Joyce, and P. J. Dobson, Surf. Sci. **103**, L90 (1981).

17. C. E. C. Wood, Surf. Sci. Lett. **108**, L441 (1981).

18. J. H. Neave, B. A. Joyce, P. J. Dobson, and N. Norton, Appl. Phys. A **31**, 1 (1983).

19. B. A. Joyce, J. H. Neave, and B. E. Watts, Surf. Sci. **15**, 1 (1969).

20. D. L. Smith and V. Y. Pickhardt, J. Appl. Phys. **46**, 2366 (1975).

21. Y. Shiraki, J. Vac. Sci. Technol. B **3**, 725 (1985).

22. A. Y. Cho and P. D. Dernier, J. Appl. Phys. **49**, 3328 (1978).

23. R. A. Betts and C. W. Pitt, *Electronics Letters* **21** (21), 960 (1985).

24. Given the recent development as well as the complex nature of the technique few good resources exist describing the fundamentals of RHEED. *Applied RHEED* (Springer, Berlin 1999) by W. Braun and the review paper cited in Ref. 25 provide an excellent overview of the technique including theory as well as applications.

25. J. E. Mahan, K. M. Geib, G. Y. Robinson, and R. G. Long, J. Vac. Sci. Technol. A **8**, 3692 (1990).

26. Although no text exists describing the fundamentals of the four-circle technique, a number of books exist describing x-ray diffraction and diffraction phenomena in general. *Elements of X-ray Diffraction* (Prentice Hall, Upper Saddle River, New Jersey 2001) by B. D. Cullity and S. R. Stock serves as a good introductory text.

27. K. J. Hubbard and D.G. Schlom, J. Mater. Res. **11**, 2757 (1996).

28. D. G. Schlom and J. H. Haeni, Mat. Res. Bull. **27**, 198 (2002).

29. J. Kwo, M. Hong, A. R. Kortan, K. T. Queeney, Y. J. Chabal, J. P. Mannaerts, T. Boons, J. J. Krajewsji, A. M. Sergent, and J. M. Rosamilia, Appl. Phys. Lett. **77**, 130 (2000).

30. J. Kwo, M. Hong, A. R. Kortan, K. L. Queeney, Y. J. Chabal, R. L. Opila, Jr., D. A. Muller, S. N. G. Chu, B. J. Sapjeta, T. S. Lay, J. P. Mannaerts, T. Boone, H. W. Krautter, J. J. Krajewski, A. M. Sergent, and J. M. Rosamilia, J. Appl. Phys. **89**, 3920 (2001).

31. J. T. Jones, E. T. Croke, C. M. Garland, O. J. Marsh, and T. C. McGill, J. Vac. Sci. Technol. B **16**, 2686 (1998).

32. J. P. Liu, P. Zaumseil, E. Bugiel, and H. J. Osten, Appl. Phys. Lett. **79**, 671 (2001).

33. D. K. Fork, F. A. Ponce, J. C. Tramontana, and T. H. Geballe, Appl. Phys. Lett. **58**, 2294 (1991).

34. Y. Kado and Y. Arita, J. Appl. Phys. **61**, 2398 (1987).

35. Y. Kado and Y. Arita in *Extended Abstracts of the 18th (1986) International Conference on Solid State Devices and Materials* (Tokyo, 1986), p. 45.

36. H. Mori and H. Ishiwara, Jpn. J. Appl. Phys. **30**, L1415 (1991).

37. H. Ishiwara, H. Mori, K. Jyokyo, and S. Ueno in *Silicon Molecular Beam Epitaxy*, edited J. C. Bean, S. S. Iyer, and K. L. Wang (Mater. Res. Soc. Proc. **220**, Pittsburgh, PA, 1991), p. 595.

38. O. Nakagawara, M. Kobayashi, Y. Yoshino, Y. Katayama, H. Tabata, and T. Kawai, J. Appl. Phys. **78**, 7226 (1995).

39. T. Tambo, K. Maeda, A. Shimizu, and C. Tatsuyama, J. Appl. Phys. **86**, 3213 (1999).

40. Y. Kado and Y. Arita in *Extended Abstracts of the 20th (1988 International) Conference on Solid State Devices and Materials* (Tokyo, 1988), p. 181.

41. H. Fukumoto, T. Imura, and Y. Osaka, Appl. Phys. Lett. **55**, 360 (1989).

42. H. Fukumoto, M. Yamamoto, and Y Osaka, Proc. Electrochem. Soc. **90**, 239 (1990).

43. K. Harada, H. Nakanishi, H. Itozaki, and S. Yazu, Jpn. J. Appl. Phys. **30**, 934 (1991).

44. S.C. Choi, M.H. Cho, S.W. Whangbo, C.N. Whang, S.B. Kang, S.I. Lee, and M.Y. Lee, Appl. Phys. Lett. **71**, 903 (1997).

45. M.-H. Cho, D.-H. Ko, Y.K. Choi, I.W. Lyo, K. Jeong, T.G. Kim, J.H. Song, and C.N. Whang, J. Appl. Phys. **89**, 1647 (2001).

46. E.J. Tarsa, J.S. Speck, and McD. Robinson, Appl. Phys. Lett. **63**, 539 (1993).

47. H. Nagata, M. Yoshimoto, T. Tsukahara, S. Gonda, and H. Koinuma in *Evolution of Thin-Film and Surface Microstructure*, edited by C.V. Thompson, J.Y. Tsao, and D.J. Srolovitz (Mater. Res. Soc. Proc. **202**, Pittsburgh, PA, 1991), p. 445.

48. M. Morita, H. Fukumoto, T. Imura, Y. Osaka, and M. Ichihara, J. Appl. Phys. **58**, 2407 (1985).

49. Y. Osaka. T. Imura, Y. Nishibayashi, and F. Nishiyama, J. Appl. Phys. **63**, 581 (1988).

50. H. Myoren, Y. Nishiyama, H. Fukumoto, H. Nasu, and Y. Osaka, Jpn. J. Appl. Phys. **28**, 351 (1989).

51. P. Legagneux, G. Garry, D. Dieumegard, C. Schwebel, C. Pellet, G. Gautherin, and J. Siejka, Appl. Phys. Lett. **53**, 1506 (1988).

52. H. Fukumoto, T. Imura, and Y. Osaka, Jpn. J. Appl. Phys. **27**, L1404 (1988).

53. H. Fukumoto, M. Yamamoto, Y. Osaka, and F. Nishiyama, J. Appl. Phys. **67**, 2447 (1990).

54. H. Fukumoto, M. Yamamoto, and Y. Osaka, J. Appl. Phys. **69**, 8130 (1991).

55. D.K. Fork, D.B. Fenner, G.A.N. Connell, J.M. Phillips, and T.H. Geballe, Appl. Phys. Lett. **57**, 1137 (1990).

56. D.K. Fork, D.B. Fenner, R.W. Barton, J.M. Phillips, G.A.N. Connell, J.B. Boyce, and T.H. Geballe, Appl. Phys. Lett. **57**, 1161 (1990).

57. D.K. Fork, F.A. Ponce, J.C. Tramontana, N. Newman, J.M. Phillips, and T.H. Geballe, Appl. Phys. Lett. **58**, 2432 (1991).

58. D.B. Fenner, A.M. Viano, D.K. Fork, G.A.N. Connell, J.B. Boyce, F.A. Ponce, and J.C. Tramontana, J. Appl. Phys. **69**, 2176 (1991).

59. W. Prusseit, S. Corsépius, M. Zwerger, P. Berberich, H. Kinder, O. Eibl, C. Jaekel, U. Breuer, and H. Kurz, Physica C **201**, 249 (1992).

60. M. Ishida, I. Katakabe, T. Nakamura, and N. Ohtake, Appl. Phys. Lett. **52**, 1326 (1988).

61. K. Sawada, M. Ishida, T. Nakamura, and N. Ohtake, Appl. Phys. Lett. **52**, 1672 (1988).

62. H. Iizuka, K. Yokoo, and S. Ono, Appl. Phys. Lett. **61**, 2978 (1992).

63. H. Wado, T. Shimizu, and M. Ishida, Appl. Phys. Lett. **67**, 2200 (1995).

64. M. Ihara, Y. Arimoto, M. Jifuku, T. Kimura, S. Kodama, H. Yamawaki, and T. Yamaoka, J. Electrochem. Soc. **129**, 2569 (1982).

65. M. Ihara, Microelectron. Eng. **1**, 161 (1983).

66. M. Mikami, Y. Hokari, K. Egami, H. Tsuya, and M. Kanamori, *Extended Abstracts of the 15th Conference on Solid State Devices and Materials* (Japan Soc. Appl. Phys, Tokyo, 1983), pp. 31-34.

67. K. Eisenbeiser, J.M. Finder, Z. Yu, J. Ramdani, J.A. Curless, J.A. Hallmark, R. Droopad, W.J. Ooms, L. Salem, S. Bradshaw, and C.D. Overgaard, Appl. Phys. Lett. **76**, 1324 (2000).

68. Z. Yu, J. Ramdani, J.A. Curless, C.D. Overgaard, J.M. Finder, R. Droopad, K.W. Eisenbeiser, J.A. Hallmark, W.J. Ooms, and V.S. Kaushik, J. Vac. Sci. Technol. B **18**, 2139 (2000).

69. M. Yoshimoto, K. Shimozono, T. Maeda, T. Ohnishi, M. Kumagai, T. Chikyow, O. Ishiyama, M. Shinohara, and H. Koinuma, Jpn. J. Appl. Phys. **34**, L688 (1995).

4-Circle X-Ray Diffractometer
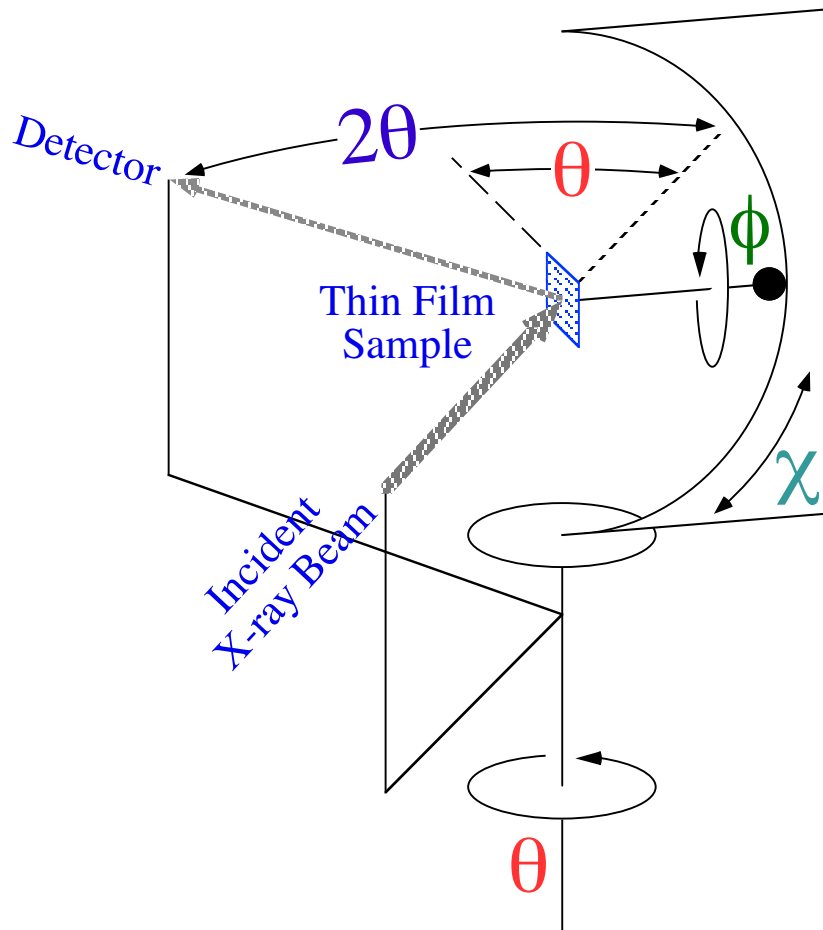
Figure 2.1: Schematic showing the geometry and angular relationships for a four circle diffraction experimental setup.
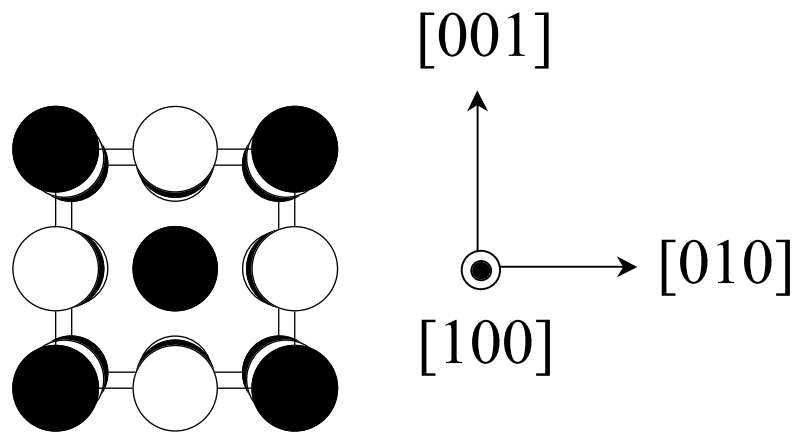
Figure 2.2: Crystal structure schematic of SrO. Strontium atoms are colored black and oxygen atoms are colored white.
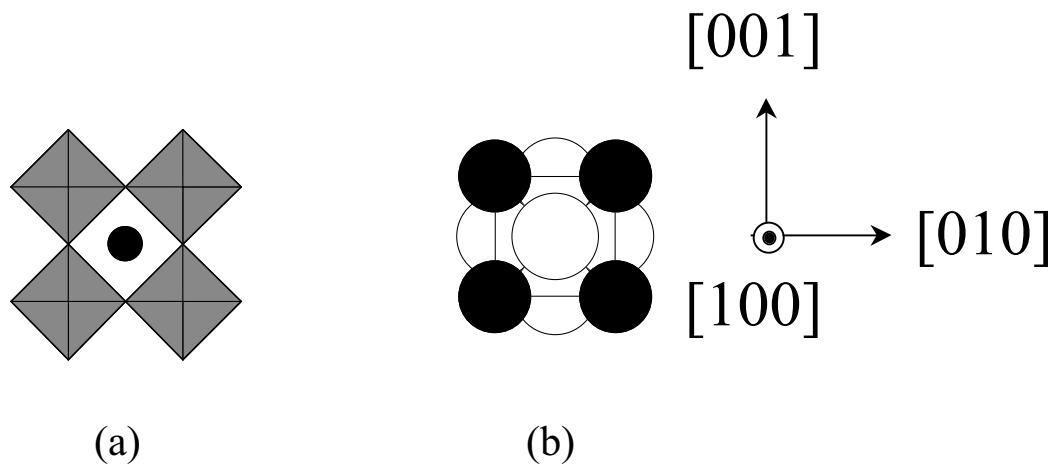
Figure 2.3: Crystal structure schematic of SrTiO$_3$. (a) Coordination polyhedra representation of the structure. Titanium atoms sit at the center of the gray octahedra. (b) Atom representation of the structure. Titanium is hidden and sits at the center of the structure. Strontium atoms are colored black and oxygen atoms are colored white.

3.0 Experimental Details

3.1 Molecular Beam Epitaxy Deposition System

The vacuum deposition chamber used to complete this work is shown

schematically in Fig. 3.1. The chamber is an EPI 930 molecular beam epitaxy deposition

system[1] modified for the growth of oxides on silicon. The vacuum system contains two

in situ diagnostic tools employed in these experiments: (1) Reflection high energy

electron diffraction (RHEED) to probe the film surface during growth and (2) a

retractable quartz crystal microbalance (QCM) used to measure mass flux in the position

of the wafer and conduct oxidation experiments. Fluxes were measured before and after

deposition and showed less than 1% fluctuation over several hours of growth. The

system allows for independent control of nine elemental sources (including the oxidant

sources) and employs computer control over furnaces, substrate heater, and shutters.

The alkaline earth metals used in this study (barium[2] and strontium[2]) were held in

titanium crucibles and deposited onto a silicon substrate by thermal evaporation from

low-temperature effusion cells. Gadolinium[3] and lanthanum[3] were held in tungsten

crucibles and deposited by thermal evaporation from high-temperature effusion cells.

Europium[3] was held in a tungsten crucible and deposited by thermal evaporation from a

low-temperature effusion cell. Aluminum[4] was held in a pyrolytic boron nitride (pBN)

crucible and deposited by thermal evaporation from a standard effusion cell. The

titanium source used in this study was from a titanium sublimation pump powered by a

precision power supply (a Ti-ball[5] source).[6] The oxidant (molecular O_2 (99.99% for all

growths) was introduced into the chamber through a needle valve connected to a tungsten tube with an outlet diameter of $\approx$ 0.6 cm a distance of $\approx$19 cm from the substrate. (This is an atomic hydrogen source[1]). Background pressures were measured with an ion gauge located on the chamber wall $\approx$ 35 cm from the substrate. The pressures given are those indicated by the ion gauge and are uncorrected for the gas species being oxygen. The base pressure for the unbaked chamber was 2×10^{-9} Torr.

Substrate temperatures above 500 °C were measured with an optical pyrometer[7] (assuming an emissivity of 0.8) aimed at the surface of the silicon substrate. Temperatures less than 500 °C were based on thermocouple measurements. The maximum deviation between thermocouple and pyrometer measurements occurred at high temperatures (e.g., at 1050 °C registered by the thermocouple, the pyrometer read 840 °C) with decreasing deviation down to room temperature. Details concerning the specific fluxes, substrate temperatures, and oxidant pressures varied depending on the material grown and the application in question. Specific details are outlined in each section.

3.2 Substrates

Films were grown on 2" and 3" diameter silicon[8] with (001) orientation held on molybdenum sample holders with pBN retainer rings. A variety of wafers were used in this study depending on both application and availability. Dopant and dopant concentration played no discernable role in the resultant structural properties. A critical role, however, was played by substrate vicinality, where higher miscut samples resulted

in generally poorer films. The bulk of the substrates used in this study were rated to
$\pm\, 0.1°$.

3.3 Other Deposition Techniques

Various other deposition techniques were also employed to make some of the
complex heterostructures described in this thesis. A combination of sol-gel processing,
magnetron sputtering, and pulsed laser deposition was used to deposit certain oxide
layers. Details concerning these growths are provided in detail in the relevant sections.
These layers were deposited at the University of Maryland under the direction of Dr.
Ramomoorthy Ramesh and at the University of Wisconsin under the direction of Dr.
Chang Beom Eom.

3.4 X-ray Analysis

The films grown in this study were characterized structurally *ex situ* using a
Picker four-circle x-ray diffractometer. The diffractometer was equipped with a copper
tube and run under typical operating conditions of 40 kV and 20 mA. Scans were
performed using Cu Kα radiation ($\lambda = 1.54$ Å) separated by means of an incident beam
graphite monochromator. Given the inability of the monochromator to distinguish the Cu
Kα radiation from the integral harmonics of this radiation, additional peaks can be seen
in some of the scans. These peaks which result from $\lambda/2$ radiation are noted in the figures
when relevant.

A scintillator counter was used as the x-ray detection source. Each of the four circle angles was controlled by means of individual stepper motors controlled electronically through the SUPER program.[9] The resolution in each of the angular space variables of 2θ, ω, ϕ, and χ are 0.15°, 0.25°, 0.35° and 1.7° respectively, as determined using a silicon single crystal standard.

Samples were mounted on a eucentric goniometer head, and a solid state laser was used to align the sample surface to the geometrical center of the diffracting sphere. Macroscopic surface alignment using this technique was accurate to ±0.2°. Samples were then aligned to specific crystallographic planes using the x-ray beam itself depending on the exact nature of the experiment.

3.5 Other Characterization Techniques

Transmission electron microscopy (TEM) was performed using a 200 kV JEOL 2010 scanning transmission electron microscope (STEM). The cross-sectional TEM specimens were prepared following standard procedures ending with ion milling in a Gatan Precision Ion Polishing System to electron transparency. All films were imaged at the University of Michigan by Wei Tian under the direction of Dr. Xiaoqing Pan.

For electrical testing samples were prepared by standard photolithography techniques followed by platinum deposition using a lift off and wet etching method. Standard ferroelectric tests were carried out using a RT 6000 tester.[10]

Piezoelectricity measurements were made with an atomic force microscope (AFM) using a conducting silicon cantilever. The measurements were made with the tip

29

of the silicon cantilever in contact with a top electrode to enable quantitative analysis and eliminate effects due to variation in tip size and shape. Capacitors were polarized using an 8V DC bias with a 2V AC bias as the drive voltage. The resultant piezoelectric deformation was probed using light deflected off the silicon cantilever and detected using a photodiode and a standard lock-in measurement. This technique was used to physically measure the capacitor displacement as a function of field and was calibrated using a single crystal quartz standard. Calibrations were made between each sample measurement. Similar techniques have been used previously to study ferroelectric and piezoelectric response in thin films.[11-18]

Electrical transport (I-V) data for high resistance samples was measured with a Keithley[19] 617 electrometer as both the voltage source and current meter. For low resistance samples, a Keithley[19] 228A was used as the voltage source and an HP[20] 3478A multimeter as the current meter interfaced to a computer for data acquisition. Samples were prepared for vertical transport measurements by depositing aluminum on the wafer backside (for backside contact) and subjected to an anneal for 30 min in air. The sample was then attached with silver paste to a copper gasket through which backside connection was made. Top electrodes were deposited as described previously. All electrical characterization was carried out at the University of Maryland under the direction of Dr. Ramamoorthy Ramesh.

---

1. Applied EPI, St. Paul, MN.

2. Aldrich-APL, Urbana, IL, 99.99% pure.

3. Alfa Aesar, Ward Hill, MA, 99.9% pure.

4. Alfa Aesar, Ward Hill, MA, 99.999% pure.

5. Varian Vacuum Products, Lexington, MA.

6. C. D. Theis and D. G. Schlom, J. Vac. Sci. Technol. A **14**, 2677 (1996).

7. Minolta / Land Cyclops 152, Osaka, Japan.

8. Virginia Semiconductor, Inc. Fredericksburg, VA.

9. Robert Fleming, AT & T Bell Laboratories.

10. Radiant Technologies, Albuquerque, NM.

11. P. Guthner and K. Dransfeld, Appl. Phys. Lett. **61**, 1137 (1992).

12. T. Tybell, C. H. Ahn, and J.-M. Triscone, Appl. Phys. Lett. **72**, 1454 (1998).

13. T. Tybell, C. H. Ahn, and J.-M. Triscone, Appl. Phys. Lett. **75**, 856 (1999).

14. P. Paruch, T. Tybell, and J.-M. Triscone, Appl. Phys. Lett. **79**, 530 (2001).

15. A. Roelofs, F. Schlaphof, U. Bottger, R. Waser, S. Trogisch, and L. M. Eng, Appl. Phys. Lett. **77**, 3444 (2000).

16. K. Franke, J. Besold, W. Haessler, and C. Seegebarth, Surf. Sci. Lett. **302**, L283 (1994).

17. T. Hidaka, T. Maruyama, I. Saki, M. Saitoh, L. A. Willis, R. Hiskes, S. A. Dicarolis, J. Amano, and C. M. Foster, Integr. Ferroelectr. **17**, 319 (1997).

18. O. Auciello, A. Gruvermann, H. Tokumoto, S. A. Prekash, S. Aggarwal, and R. Ramesh, MRS Bull. **23**, 33 (1998).

19. Keithley Instruments, Inc., Cleveland, OH.

20. Hewlett Packard, Inc., Palo Alto, CA.
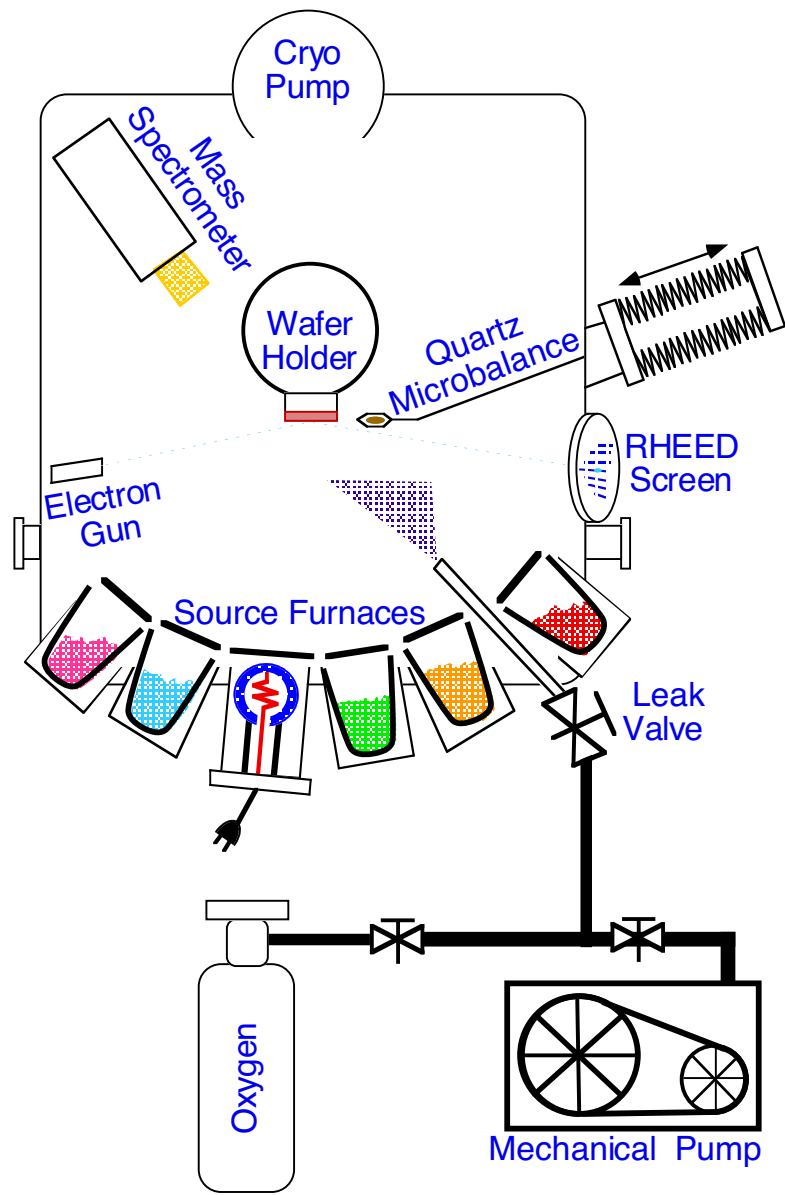
Figure 3.1: Schematic of the MBE deposition chamber used for the growth of epitaxial oxides on silicon.

4.0 Kinetics of Oxidation

As outlined in Chapter 2, the growth strategy explored in this work falls under the classification of growth in a low temperature / excess oxygen regime. Although this regime benefits from the sluggish kinetics for silicon oxidation, the drawback is the potential for sluggish oxidation kinetics of the deposited metal species as well. Consequently, assessing kinetic barriers to oxidation of the species being supplied to the substrate is critical in the successful growth of oxides on silicon. As a result, the threshold for oxidation of the metal systems, i.e., the absolute minimum pressure where one can oxidize the metal and grow a film, represents an important process parameter.

Oxidation of the metallic species can be a significant roadblock for growth of these oxides on silicon in an MBE regime. One solution is to use some type of activated oxygen species. For example, solid oxygen sources,[1] oxygen plasmas,[2-4] and ozone[5] have all been used to promote oxidation in oxide film growth while lowering the overall chamber pressure. Although highly effective for growing on oxide substrates, use of an activated oxidizing species would optimally be avoided when growing on silicon. One would like to fully oxidize and grow at as low a temperature and as low an oxygen pressure as possible, oxidizing the deposited species, while avoiding oxidation of the substrate.

This chapter addresses the issues related to oxidation kinetics and describes a series of experiments utilizing the *in situ* QCM on the MBE examining both the threshold for oxidation of relevant metals which form silicon compatible oxides as well as oxidation catalysis to promote oxidation in some poorly oxidizing metal systems.

4.1 QCM Experiments – General Description

In each experiment the mass accumulation rate as measured by the QCM was plotted (e.g., Figs. 4.1-4.7) as a function of time as a solid, heavy line. During the course of these depositions the background oxygen pressure in the chamber was increased at various intervals, and the changes in the mass accumulation rate were recorded. The labeled, solid dark lines indicate the positions corresponding to the mass accumulation rate of the pure metal and fully-oxidized metal oxide. (The significance of the higher oxidation state line in the barium plot is addressed in the next section.) Sources were left to equilibrate for two hours (i.e., the appropriate shutter was opened and pure metal in vacuum was deposited on the QCM) before the collection of data in the plots shown here. This equilibration was completed to eliminate any effects due to transients associated with opening of the source shutter and the accompanying small changes in temperature at the QCM (during the onset of deposition) which can have effects on the measured QCM rates. Small transients upon the introduction of oxygen into the system can be seen in some of the plots (titanium, lanthanum, and barium) due to the exothermic oxidation reaction which can cause small changes to the QCM temperature and resultant rate reading. Small transients can also result due to oxidation of material previously deposited on the QCM during the collection of the data set. In all cases, the effect of this transient was eliminated by waiting the appropriate amount of time until the steady state condition was reached. Only data points recorded once the steady state rate was reached

were used in the quantitative calculations. Experiments were conducted with metal deposition rates between 10^{13}-10^{14} atoms/cm^{2}s.

4.2 Single Species Oxidation

The plots showing oxidation data for individual metallic species are shown in Figs. 4.1-4.7. As one might expect, different elements exhibited different oxidation behavior. This can be viewed more easily if the data is plotted as the oxygen to metal ratio in the metal oxide as a function of oxygen partial pressure. Figure 4.8 shows such a plot for all the elemental species examined in this study for ease of comparison. The results of these oxidation studies demonstrate three important results: (1) the alkaline earth oxides are optimal candidates for growth on silicon from an oxidation perspective, i.e., barium and strontium can be fully oxidized at partial pressures in the 10^{-9} to low 10^{-8} Torr range, (2) similar metals oxidize oxidize similarly (i.e., the rare earths behave similarly and the alkaline eraths behave similarly) and (3) full oxidation of other species (such as aluminum) can become a limiting factor if one wants to oxidize the metal species without oxidizing the silicon underneath and potentially eliminating the possibility of growing an epitaxial film. (The bare silicon substrate, for example, will form 0.5 ML of oxide at room temperature upon exposure to 1×10^{-6} Torr O_2 for less than ten seconds).[6] A strategy developed to overcome this critical limitation is described in the next section.

The general concept of the influence of a metal's work function on the oxidation of the metallic species has been previously noted by Braaten *et al*.[7] A summary of the

single element oxidation behavior presented in Fig. 4.9 confirms this relationship. Figure 4.9 shows a plot of "ease of oxidation" for the different metals studied. Here, ease of oxidation is defined as the pressure at which the metal is at half of its fully oxidized oxidation state (i.e., where deposited strontium is at an average oxidation state of 1+). (Some apparent exceptions to this general rule can exist (e.g., the case of titanium), and for potentially other transition metals that can exhibit multiple oxidation states where the low oxidation state may be easily achieved, but the fully oxidized condition may be difficult to attain. For the purposes of this plot, the barium and strontium are considered to be 2+ in their fully oxidized state, the aluminum, europium, gadolinium, and lanthanum to be 3+, and the titanium to be 4+).

It should be noted that for growth in the low temperature, excess oxygen regime in which these films are grown, it is the system kinetics that will ultimately determine failure or success. The oxidation of aluminum serves as a prime example, for while aluminum oxide is thermodynamically quite stable, the kinetic barrier to oxidation will limit one's ability to form the oxide in the first place.

4.2.1 Notes Concerning Individual Plots

The following sections describe brief notes concerning the individual oxidation experiments.

4.2.2 Oxidation of Strontium, Europium, Aluminum, and Titanium

These four species behave as expected and with oxidation or nearly full oxidation achieved in the pressure window examined in this study (i.e., pressures reasonable using the MBE technique). Titanium could not be entirely oxidized to a 4+ state at pressures needed to both maintain an MBE deposition regime as well as preserve the source material. However, reaching a 3+ state was achieved at pressures conducive for the growth of epitaxial oxides on silicon.

4.2.3 Oxidation of Barium

Barium showed an oxidation state higher than the 2+ state typically found in group II metals even in depositions at low pressures. This is not unexpected, since barium has also been shown previously to exist in a 4+ state in the pressure regime in which these experiments were conducted.[8] Figure 4.10 shows a temperature-pressure phase diagram for the Ba-BaO-BaO$_2$ system. The experimental window is highlighted on the figure.[9,10]

4.2.3 Oxidation of Lathanum and Gadolinium

Examination of the lanthanum and gadolinium oxidation charts seemingly show oxidation states higher than the 3+ state normally associated with these metals. Thermodynamically higher oxidation states in these metals are not expected. For these materials, this can be explained as noise in the QCM signal. The noise level for La can

be seen on Fig. 4.8 as an error bar, which is representative of the magnitude of experimental noise for all the species studied in this thesis.

4.3 Multiple Species Oxidation and Oxidation Catalysis

In addition to single element oxidation, the oxidation of codeposited metal species was investigated. The data are shown in Figs. 4.11-4.15 for strontium/titanium, barium/titanium, lanthanum/aluminum, barium/strontium, and lanthanum/strontium/aluminum respectively. These experiments were conducted in a similar fashion as those described in Figs. 4.1-4.7 with oxygen introduced into the deposition chamber once the deposition of all the metal species had begun. Although oxide MBE growth strategies (shuttered layer-by-layer, block-by-block, codeposition) have been investigated for years, fundamental questions still exist concerning the optimal deposition technique. This experiment examines the oxidation behavior of codeposited metals in an MBE environment.

The motivation for looking at these specific oxidation studies in the stoichiometries investigated stems from ternary and quaternary compounds of potential interest for growth on silicon. Each of these systems, strontium/titanium ($SrTiO_3$), barium/titanium ($BaTiO_3$), lanthanum/aluminum ($LaAlO_3$), barium/strontium ($(Ba,Sr)O$ – the alkaline earth lattice matched to silicon at room temperature), and lanthanum/strontium/aluminum ($LaSrAlO_4$), represents an oxide that is either thermodynamically stable in contact with silicon or (in the case of the titanates) can be made stable if the interfacial layer is the alkaline earth layer of the structure.

Careful examination of the oxidation behavior reveals that certain difficult to oxidize species can be fully oxidized when codeposited with easily oxidized species at pressures much lower than with the deposition of the pure metal alone. This behavior can be seen most dramatically in the example shown in Fig. 4.16. The plot in Fig. 4.16 shows the oxidation behavior for an 80% aluminum (species difficult to oxidize) / 20% strontium (species easy to oxidize) mixture. By plotting this data (Fig. 4.17) in a similar fashion to the data plotted in Fig. 4.8 the results become more apparent. The aluminum species has been fully oxidized in the presence of a small amount of strontium at pressures an order of magnitude lower than just the aluminum metal alone.

The oxidation behavior witnessed here has been seen previously with other systems, though the use of an alkali metal catalyst and has been attributed to surmounting kinetic barriers to oxidation.[11-13] Similar behavior is seen here with the alkaline earth metals. In their previous work on alkali metals,[11] Braaten *et al.* attribute this type of catalytic behavior to the ability of an easily oxidized metal to increase the rate of dissociation of oxygen at the substrate surface. These results also support the trend that lower work function materials result in higher oxygen incorporation.[11] The analogous results are demonstrated here for the first time with the alkaline earths.[14]

The results of this study are fortuitous, since the use of a small amount of codeposited alkaline earth metal may allow the oxidation of a host of difficult to oxidize species. This thesis focuses primarily on the deposition of the more easily oxidized metals (alkaline earths and rare earths) because of their thermodynamic stability with silicon. However, as more complex oxides are investigated, oxidation will remain a key issue and play a critical role in the successful growth of these materials.

1. R. A. Stall, J. Vac. Sci. Technol. B **1**, 135 (1983).

2. D. G. Schlom, J. N. Eckstein, E. S. Hellman, C. Webb, F. Turner, J. S. Harris, Jr., M. R. Beasley, and T. H. Geballe, in *Extended Abstracts, High-Temperature Superconductors II*, (D.W. Capone, II, W.H. Butler, B. Batlogg, and C.W. Chu, eds.) pp. 197-200, Materials Research Society, Pittsburgh (1988).

3. R. J. Spah, H. F. Hess, H. L. Stormer, A. E. White, and K. T. Short, K.T., Appl. Phys. Lett. **53**, 441 (1988).

4. D. G. Schlom, J. N. Eckstein, E. S. Hellman, S. K. Streiffer, J. S. Harris, Jr., M. R. Beasley, J. C. Bravman, T. H. Geballe, C. Webb, K. E. von Dessonneck, and F. Turner, Appl. Phys. Lett. **53**, 1660 (1988).

5. D. D. Berkley, B. R. Johnson, N. Anand, K. M. Beauchamp, L. E. Conroy, A. M. Goldman, J. Maps, K. Mauersberger, M. L. Mecartney, J. Morton, M. Tuominen, and Y-J. Zhang, Appl. Phys. Lett. **53**, 1973 (1988).

6. E. G. Keim, L. Wolterbeek, and A. Van Silfhout, Surf. Sci. **180**, 565 (1987).

7. N. A. Braaten, J. K. Grepstad, S. Raaen, and S. L. Qui, Surf. Sci. **250**, 51 (1991).

8. T. Onishi, M. Yoshimoto, G. H. Lee, T. Maeda, and H. Koinuma, J. Vac. Sci. Technol. A **15**, 2469 (1997).

9. The curves were calculated using thermodynamic data from J. Phys. Chem. Ref. Data **16**, 419 (1987).

10. This figure is adapted from a figure in Ref. 8.

11. N. A. Braaten, J. K. Grepstad, S. Raaen, and S. L. Qui, Surf. Sci. **250**, 51 (1991).

12. P. Soukiassian, T. M. Gentle, M. H. Bakshi, and Z. Hurych, J. Appl. Phys. **60**, 4339 (1986).

13. Y. Huttel, E. Bourdie, P. Soukkiassian, P. S. Mangat, and Z. Hurych, Appl. Phys. Lett. **62**, 2437 (1993).

14. J. Lettieri, J. Rodriguez Contreras, V. Vaithyanathan, and D. G. Schlom, unpublished.
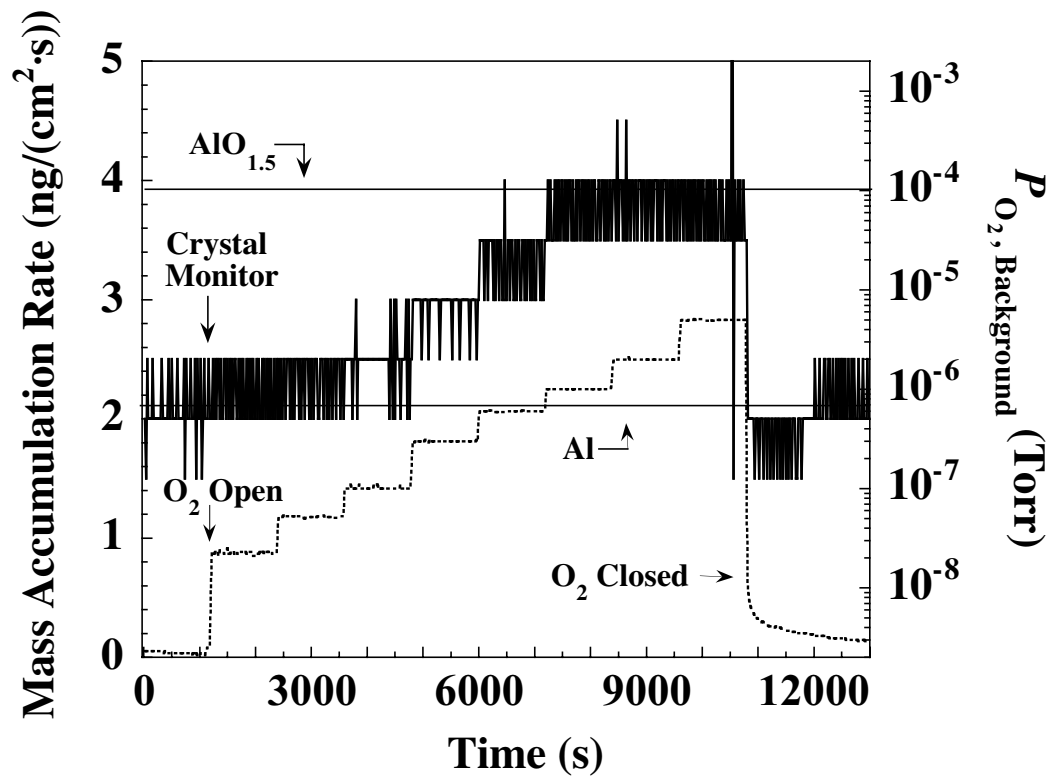
Figure 4.1: Oxidation behavior of aluminum metal as a function of oxygen partial
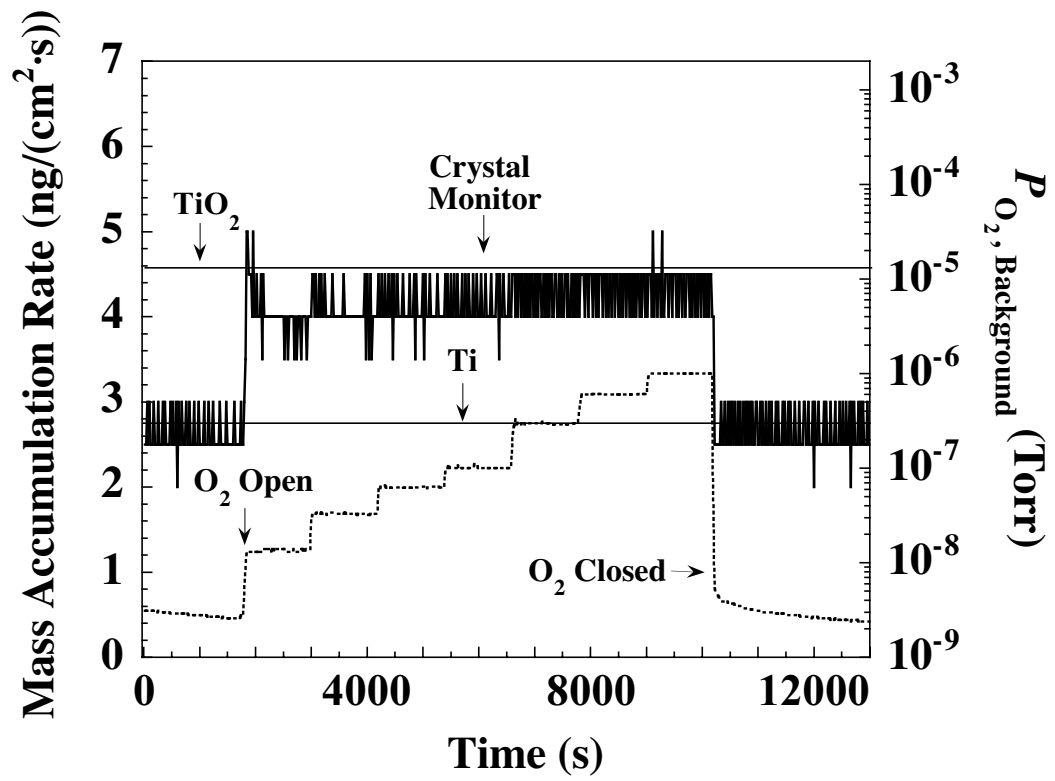
pressure.

Figure 4.2: Oxidation behavior of titanium metal as a function of oxygen partial pressure.
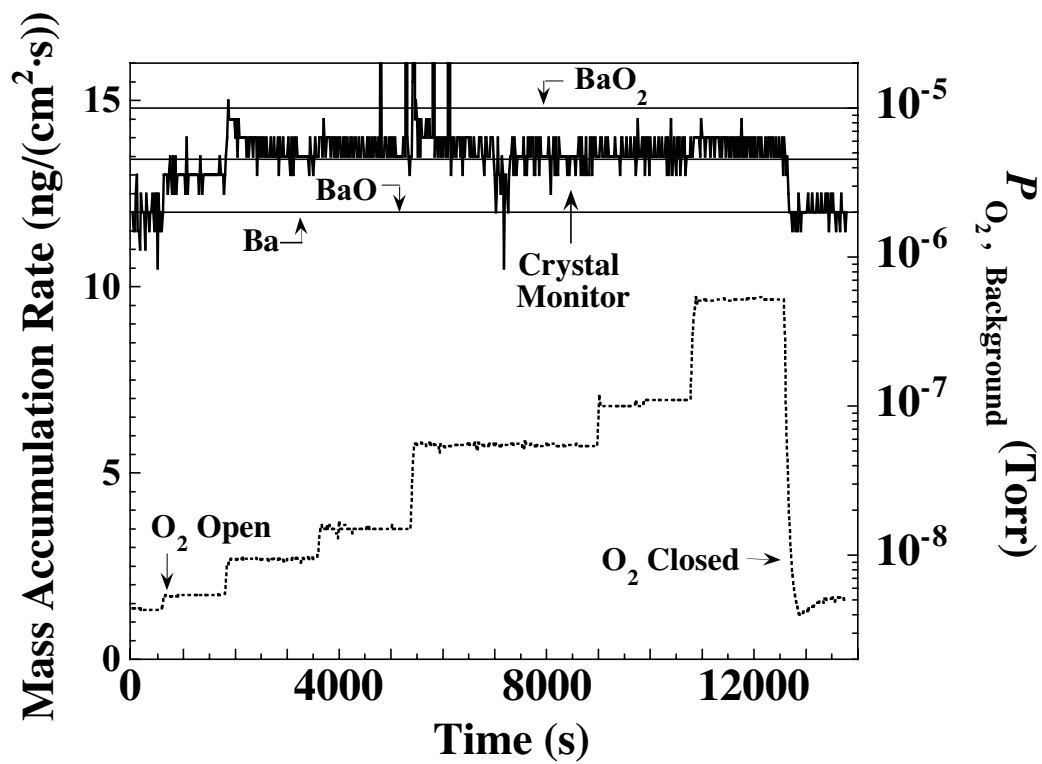
Figure 4.3: Oxidation behavior of barium metal as a function of oxygen partial pressure.
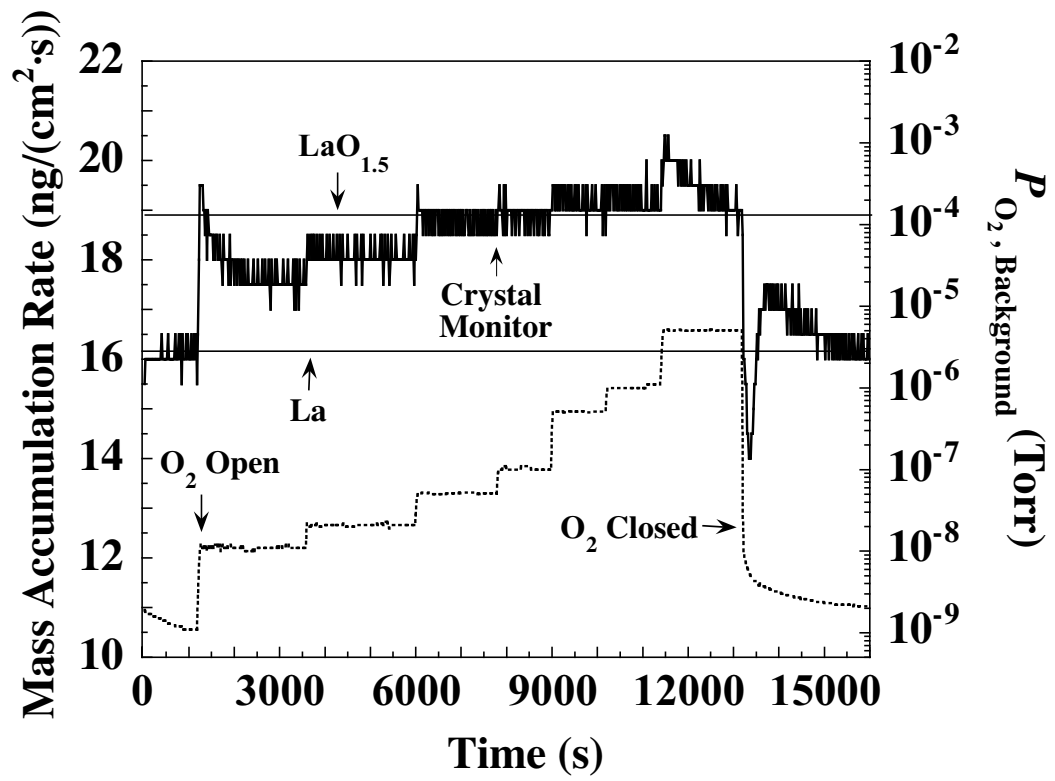
Figure 4.4: Oxidation behavior of lanthanum metal as a function of oxygen partial
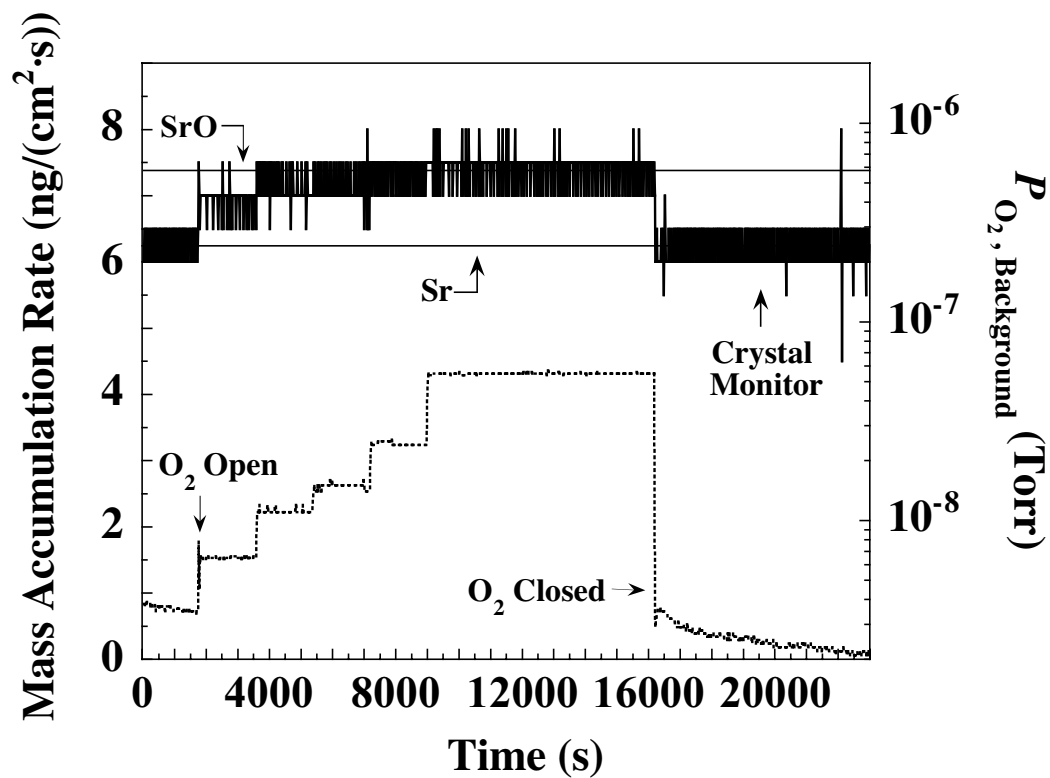
pressure.

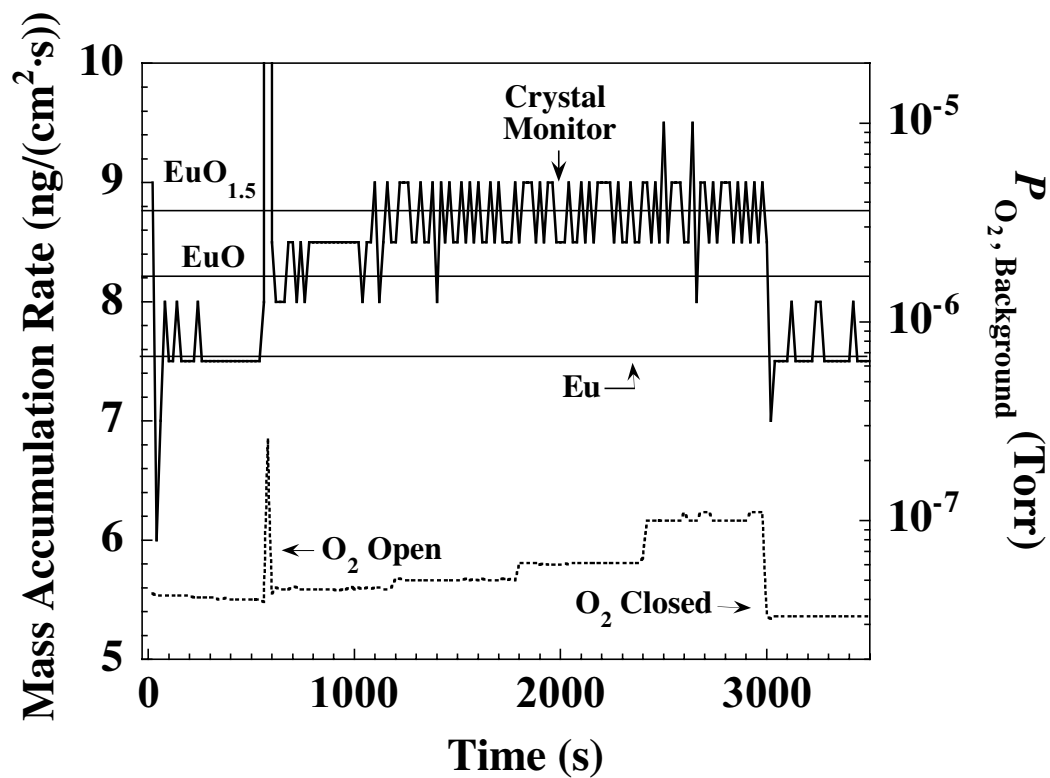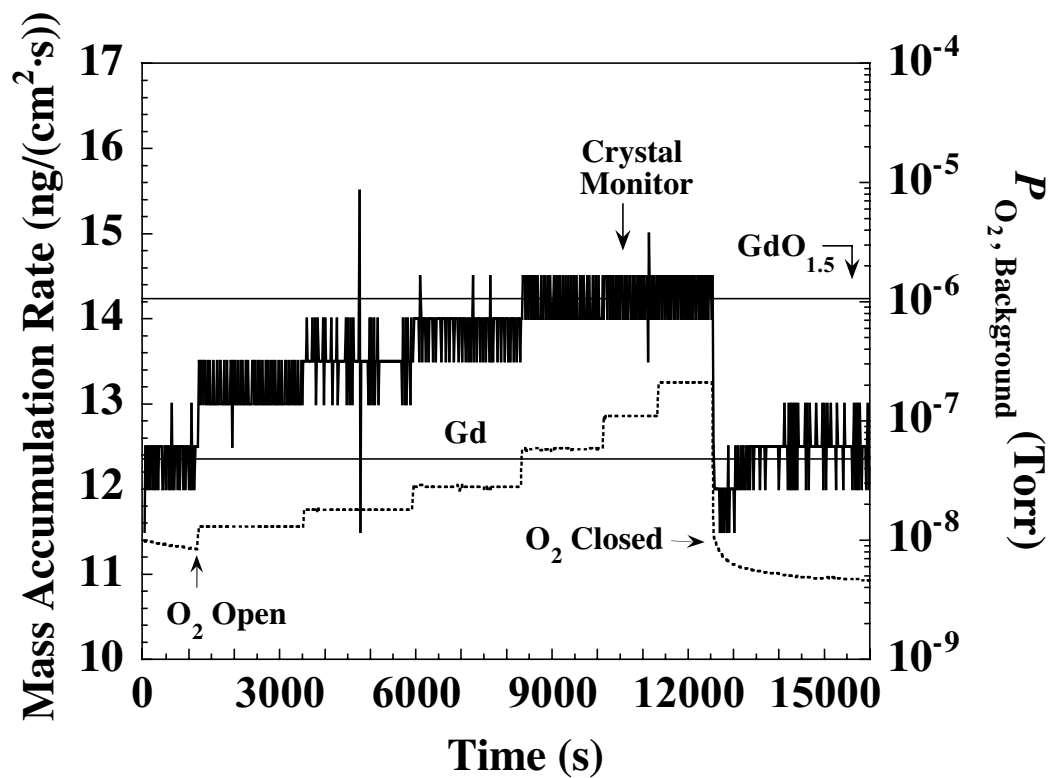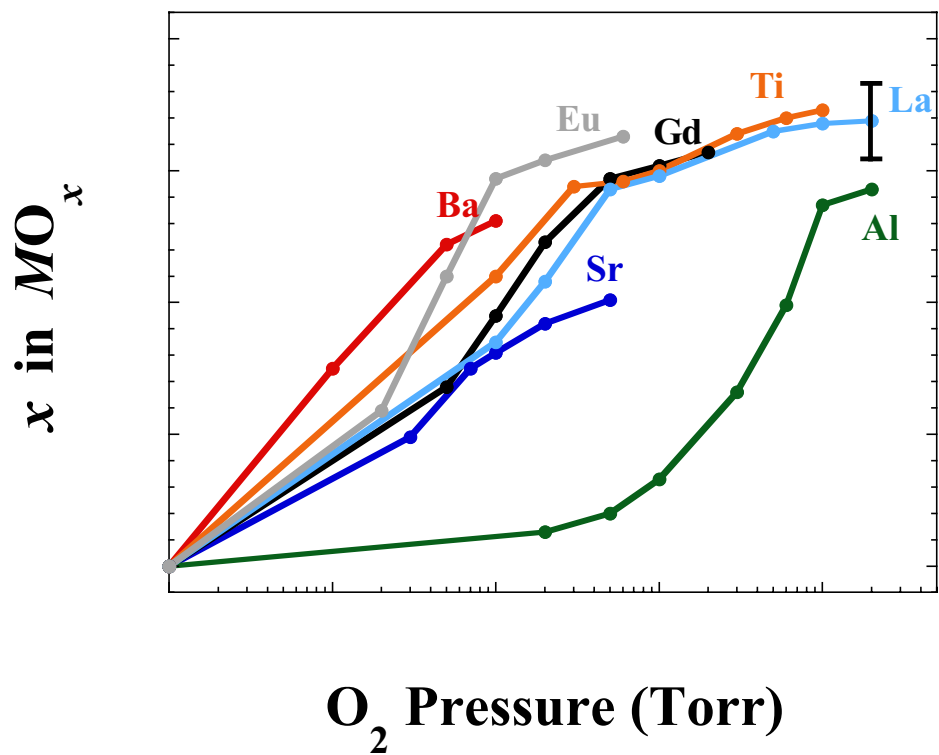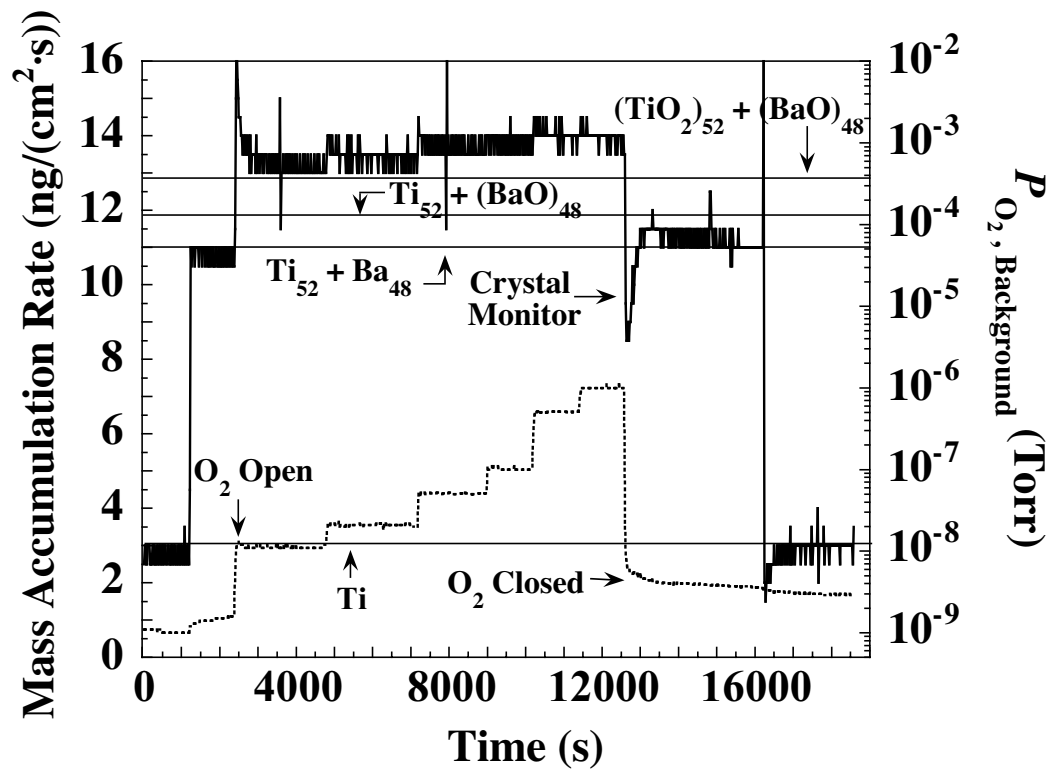Figure 4.5: Oxidation behavior of strontium metal as a function of oxygen partial pressure.

Figure 4.6: Oxidation behavior of europium metal as a function of oxygen partial pressure.

Figure 4.7: Oxidation behavior of gadolinium metal as a function of oxygen partial pressure.

x in MO$_x$

O$_2$ Pressure (Torr)

Eu   Ti   La   Gd   Ba   Sr   Al

Figure 4.12: Oxidation behavior of codeposited barium and titanium as a function of oxygen partial pressure.
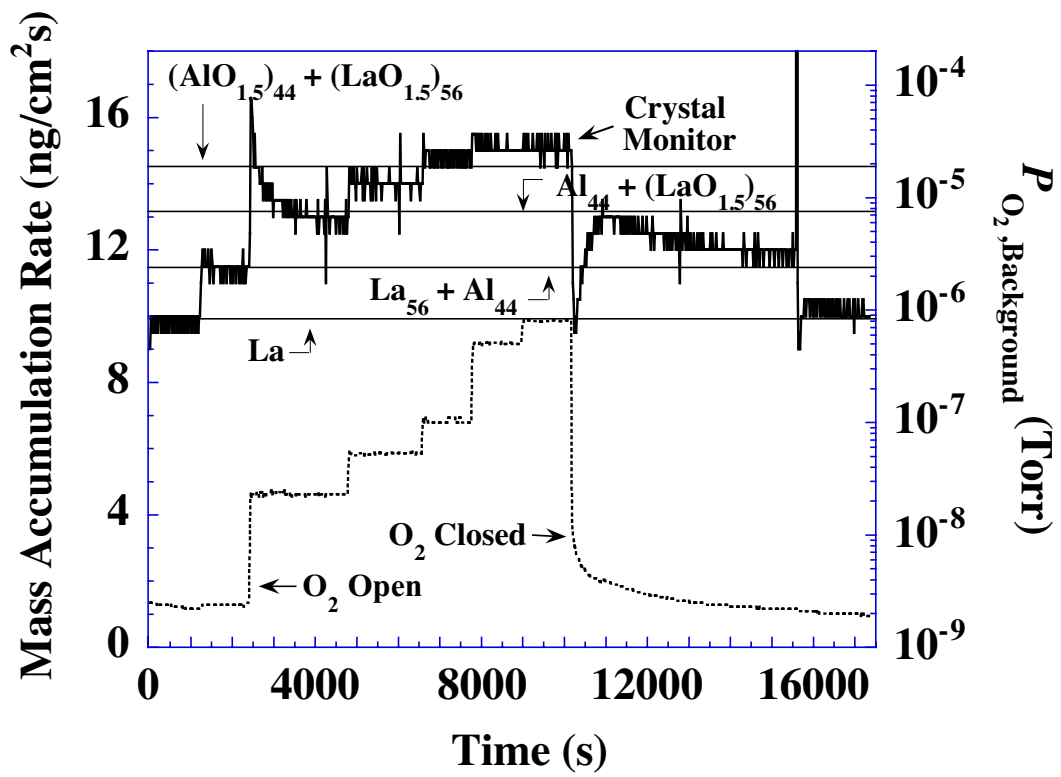
Figure 4.13: Oxidation behavior of codeposited lanthanum and aluminum as a function
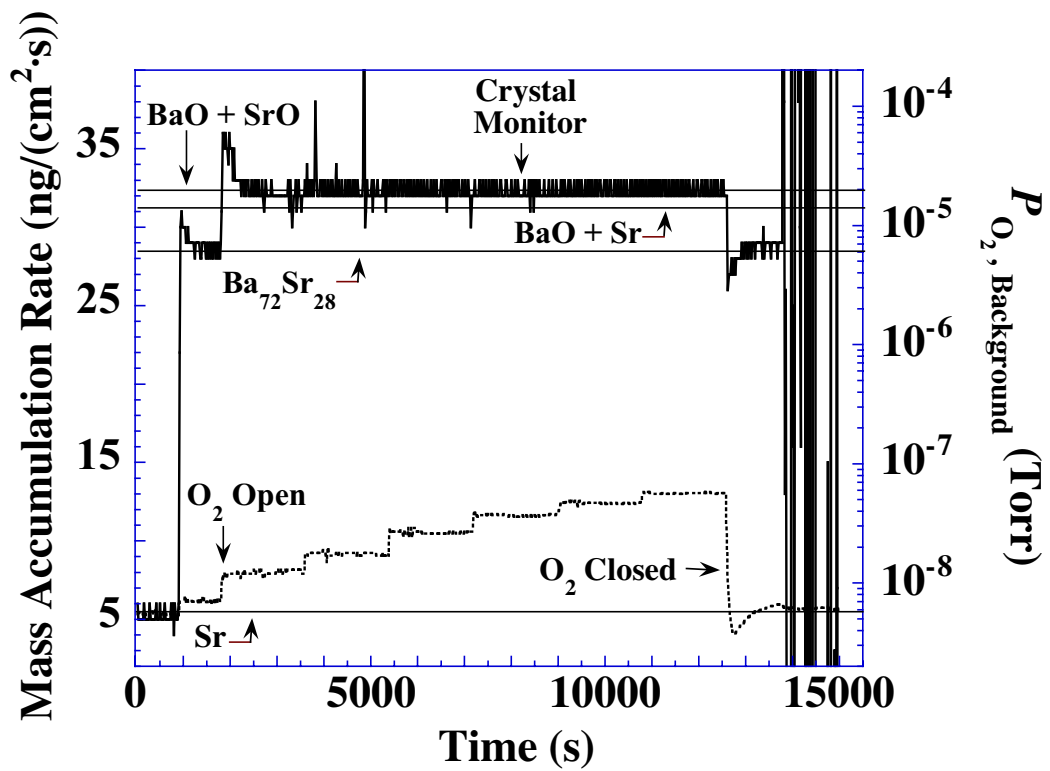
of oxygen partial pressure.

Figure 4.14: Oxidation behavior of codeposited barium and strontium as a function of
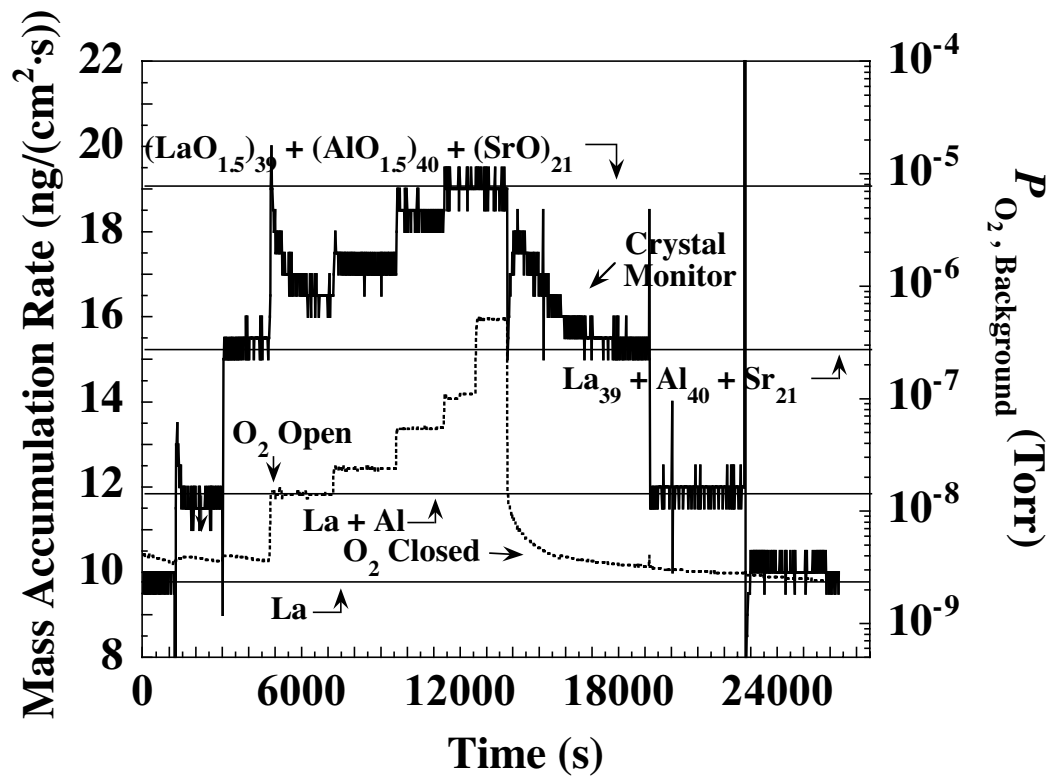oxygen partial pressure.

Figure 4.15: Oxidation behavior of codeposited lanthanum, aluminum, and strontium as a function of oxygen partial pressure.
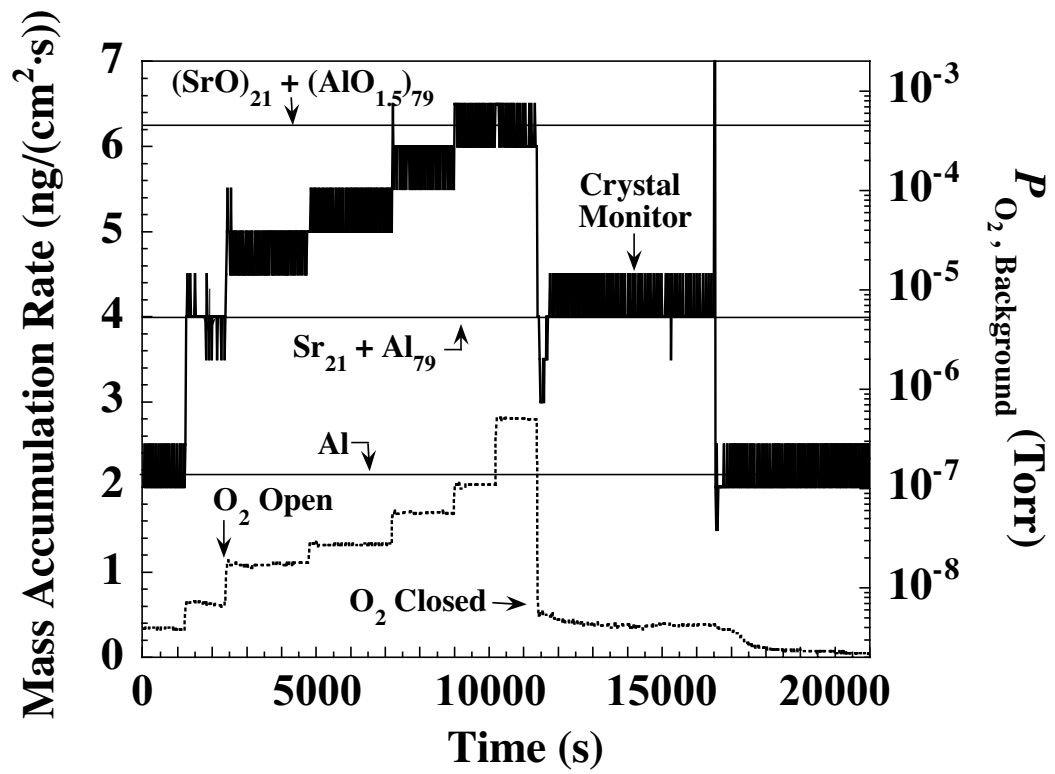
Figure 4.16: Oxidation behavior of codeposited strontium and aluminum as a function of oxygen partial pressure.
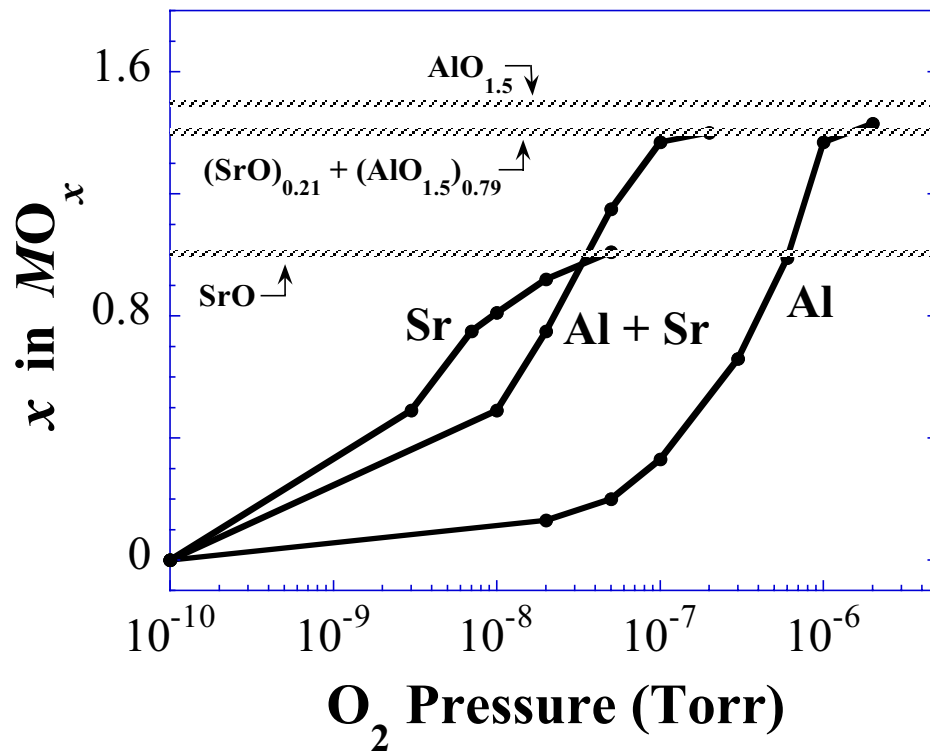
Figure 4.17: Oxidation behavior of pure strontium metal, pure aluminum metal, and codeposited aluminum and strontium in an ~ 80:20 ratio.

5.0 Alkaline Earth Oxides on Silicon

Given the favorable oxidation kinetics and the thermodynamic stability addressed in the previous chapters, alkaline earth oxides serve a logical choice for epitaxial growth on silicon. This chapter further describes the crucial and advantageous structural aspects of the alkaline-earth oxide/silicon system, which enable these materials to grow in an epitaxial and highly crystalline manner. The step-by-step transition from the silicon to the alkaline earth oxide is described in detail, with emphasis placed on the favorable interface stability, structural, and strain considerations for each stage of the growth.

5.1 RHEED Evolution

One of the easiest ways to describe the transition from silicon to alkaline earth oxide is by examining the RHEED evolution through this process. Figure 5.1 shows various paths taken to effect the transition from silicon to alkaline earth oxide. RHEED images along the [110] azimuth of silicon at different stages of the growth processes illustrated in Fig. 5.1 are shown in Fig. 5.2(a-h). These figures will be referred to extensively over the next few sections to describe the transition and growth of the oxide. The variation in process temperature and alkaline-earth metal dose as outlined in Fig. 5.1 demonstrate that some latitude does exists in achieving an epitaxial alkaline-earth oxide on silicon. While some variation can be seen in the RHEED images in Fig. 5.2, the key elements (clean, reconstructed silicon surface, formation of a submonolayer silicide, and

metal overlayer) are common to paths that will ultimately yield epitaxial oxides. These steps are described in detail in the next sections.

5.1.1 Reconstructed Silicon

Since the goal of this work is achieving an abrupt crystalline interface, beginning the growth process with a clean, crystalline silicon surface is of critical importance. Excessive carbon contamination can lead to the formation of SiC, which will severely degrade the epitaxy in the layers that follow.[1] Figure 5.2(a) shows a RHEED image of a reconstructed, double-domain (2×1) Si surface, which represents the first step of this multistep growth. To obtain this surface, a silicon wafer was put under an ultraviolet (UV) lamp for one minute (with the UV lamp creating a localized ozone atmosphere) as an ozone treatment, and then loaded into the deposition chamber and heated in vacuum to 840 °C for 20 minutes. All amorphous SiO_2 on the substrate surface, which could hinder epitaxy must be eliminated prior to growth, and the (2×1) Si that results provides an excellent template for subsequent epitaxial growth.

5.1.2 Silicide Formation

The second stage of the growth process is the deposition of the alkaline-earth metal (in this example strontium) and the formation of a submonolayer silicide at ~700 °C (see PATH 1 in Fig. 5.1). At 1/6 monolayer (ML) of deposited strontium dose[2] the RHEED pattern evolves into a $3 \times$ reconstruction. At 1/2 ML of deposited strontium

dose, the RHEED pattern returns to a 2 × pattern with maximum intensity (Figs 5.2(b)

and 5.2(c), respectively). Although the true composition of the surface yielding the 1/2

order streaks remains an unresolved issue[3,4] and the determination of its exact nature

remains a formidable task,[5,6] the character of the surface no longer resembles that of pure

silicon, nor that of strontium metal.[7,8] In fact, the nomenclature itself of this layer

remains a debatable issue. Previous work has predicted, that although a Sr-Si bond

exists, the properties of such a layer do not resemble that of a bulk silicide, but rather that

of a chemisorbed strontium on a silicon surface.[9] The semantics may or may not be a

moot point, however, for ease of description in this thesis, this layer will be referred to as

the "submonolayer silicide."

The formation of the submonolayer silicide is a critical step in the process, and no

success was achieved in situations where a silicide is not first grown. The complete role

of this layer is multiple and complex. Principally, it forms an excellent template (in

terms of lattice constant) for the subsequent growth of the oxide. Additionally, this

silicide structure (based on RHEED observation) exhibits a much higher resistance to

oxidation that the silicon surface alone, in agreement with Ref. 7. (The ultimate chemical

nature of this interfacial silicide layer upon exposure to oxygen is discussed in Sec. 5.1.4)

Finally, the formation of the submonolayer silicide allows the next step of the transition,

the deposition of an alkaline-earth metal overlayer.

As stated previously, there is a dosage window in terms of deposited strontium

that leads to epitaxial oxide growth. This can be seen by following the dotted path

(PATH 2) on Fig. 5.1 where instead of 1/2 ML, a 1/4 ML silicide is grown. Although the

RHEED evolution is slightly different, the deposition of the 1/4 ML presents a viable path to epitaxial growth (Figs. 5.2(f-h)).

5.1.3 Alkaline Earth Metal Deposition

For the next step of the transition, (see Fig. 5.1) the substrate temperature is cooled considerably and additional alkaline-earth metal is deposited until the RHEED pattern in Fig. 5.2(e) is observed which is indicative of an ordered $3 \times$ structure. Slight changes in substrate temperature will have a significant effect on the quality of this ordered strontium metal overlayer, which can be observed even when deposited at room temperature. The pattern in Fig. 5.2(e) shows a RHEED image resulting from the deposition at 120 °C. The quality of this $3 \times$ reconstruction will not limit one's ability to grow epitaxial alkaline-earth oxide in the next step. The critical idea, however, is that this heteroepitaxial stack now consists of the silicon substrate, submonolayer silicide and submonolayer metal overlayer. In many other systems (including the rare earths) similar behavior is not observed.[10] Often the further deposition of metal will result in the formation of a thick silicide layer even at room temperature.[11] Formation of a thick silicide in many cases can lead to decreased crystalline quality and multiple film orientations. Additionally, in many applications (i.e., where a field effect between the overlying dielectric or ferroelectric and underlying silicon is desired) the formation of a thick silicide should be avoided to prevent the screening of the desired field effect by this intermediate silicide layer. The formation of a stable submonolayer silicide and

subsequent metal overlayer, which is a relatively uncommon phenomenon, makes alkaline-earth metals and oxides so amenable to this process. This metal overlayer, which plays a role in the initial stages of oxidation will be explained in more detail in the next section.

As with the previous layer, the true nature of the layer in this third step of the deposition is not definitively clear. Conclusive determination of the character of this layer as a metal is ambiguous at best, even through the use of high-resolution x-ray photoelectron spectroscopy.[5] However, based on previous low energy electron diffraction (LEED) studies[12] and our own work looking at oxidation of this layer, we believe it to be consistent with a physisorbed metallic strontium overlayer or (again, for ease of description) a "submonolayer metal." Furthermore, epitaxial alkaline-earth oxide can be obtained over a range of strontium dosage at this stage. An epitaxial oxide has been grown for deposited strontium doses ranging from 3/8 to 1 ML (although the 3 × reconstruction will disappear), which gives credence to the idea that this layer is, in fact, a metal which gets incorporated into the film during the onset of oxidation in the next step of the process. (Potentially an even thicker strontium metal layer could be successful, however, we have explored only to 1 ML of deposited strontium dose).

5.1.4 Oxidation

The general growth procedure that has yielded consistently high quality results has been to slowly increase the partial pressure of oxygen into the chamber to a background pressure of approximately 5×10^{-9} Torr and begin depositing the alkaline

62

earth metal while simultaneously raising the oxygen pressure to approximately 1-3×10^{-8} Torr. One of the functions of the deposited metal overlayer described in the previous section is to help ease the transition into the formation of the oxide. This can be seen through inspection of the RHEED as the $3 \times$ metal overlayer evolves to a $1 \times$ while the oxygen partial pressure is increased to 5×10^{-9} Torr. A continued increase of the oxygen pressure in this step or beginning the deposition of the alkaline earth metal too slowly will result in diminished epitaxial quality and some amorphous content, which can been seen in the RHEED. When the procedure is implemented in the correct pressure regime the patterns in Figs. 5.3(a) and 5.3(b) result. The patterns shown in Fig. 5.3 are from the growth of lattice matched $Ba_{0.70}Sr_{0.30}O$ on (001) silicon (lattice matching and solid solution of the alkaline-earth oxides are addressed in the next section).

Questions still exist concerning the ultimate composition and structure of the interfacial silicide upon exposure of the silicon/silicide/metal stack to oxygen. Wang *et al*. have predicted based on first principles calculations the transformation of the silicide layer to a silicate in the presence of oxygen.[4] The stability of this layer in an oxygen environment might suggest a transformation to a silicate. Whereas an alkaline-earth metal / silicon interface might lead to promoted oxidation of the underlying silicon[13,14] (through the catalytic behavior described previously), the formation of a silicate could serve as a protective layer and stem the formation of amorphous SiO_2. As with the silicide, questions of nomenclature exist, and the most correct terminology for the interface may be described as "a layer consisting of silicon, strontium, and oxygen," however the true chemistry is still debated.

5.2 Lattice Matching and RHEED Oscillations

Besides the advantageous oxidation behavior described in the Chapter 4, alkaline-earth oxides are able to grow epitaxially at extremely low temperatures due to the highly ionic nature of their bonding.[15] For example, epitaxial growth of MgO has previously been demonstrated at temperatures down to 140 K.[16] The patterns shown in Fig. 5.3 were taken for films grown at room temperature. Reduction of the growth temperature not only minimizes the potential for diffusion and interfacial reaction, but also minimizes the possibility of unwanted oxidation of the silicon substrate. From a process control and repeatability perspective, this third regime for the growth of epitaxial oxides on silicon mentioned in Section 2.3.2 is the best. The extremely low temperatures at which the alkaline earth oxide layer may be grown epitaxially makes this desired regime accessible for the growth of lattice-matched (Ba,Sr)O epitaxial layers on silicon.

Another critical advantage to the alkaline-earth oxides is the ability to tune the lattice constant over a wide range of values utilizing solid solutions of different alkaline-earth oxide constituents. Given a lattice constant of silicon of 5.43Å, the solid solution of $Ba_{0.72}Sr_{0.28}O$ results in a perfectly lattice-matched oxide. Despite the significant miscibility gap known to exist in the BaO-SrO system,[17] (the phase diagram is shown in Fig. 5.4) work by Hellman *et al*. previously demonstrated complete solid solution for SrO-CaO thin films (another alkaline earth oxide system with a complete miscibility gap in bulk form) grown on MgO at room temperature.[18] Enhanced miscibility in epitaxial films vs. bulk is well established in other systems,[19,20] including oxides.[21] Here similar

results are seen (complete solid solution) for the growth of $Ba_xSr_{1-x}O$ on silicon. This solid solubility allows for the tuning of the lattice constant of the oxide to be either perfectly latticed matched to the silicon to create a coherent interface, or optionally modified to engineer an intentional strain which has been shown to modify the properties of epitaxial layers in other systems.[22,23] The implications and differences between growing a lattice-matched oxide and a non-lattice-matched oxide can be seen clearly in the RHEED intensity oscillations during growth. Figures 5.5 and 5.6 show RHEED intensity oscillations of the specularly-reflected spot (along the [110] azimuth of silicon) for pure SrO and lattice-matched (Ba,Sr)O, respectively, grown on (001) silicon at 25 °C. The oscillations for the mismatched SrO show markedly decreasing intensity and dampening of the oscillations, in direct contrast the oscillations shown in Fig. 5.6. The sharp decrease is due to relaxation of the mismatched SrO at a very small critical thickness; analogous RHEED oscillations have been reported for mismatched compound semiconductor heteroepitaxy.[24]

Corroborating data can be seen by looking at the diffraction patterns themselves at different thicknesses during the growth. Figures 5.7 and 5.8 show RHEED images taken along two azimuths ([110] and [100], respectively) at 2 ML and 5 ML of SrO coverage. The pattern at 2 ML of SrO (along the [110] azimuth) show sharp spots on a ring as would be expected for a coherent interface and flat surface. At 5 ML of coverage, the spots extend into diffuse streaks. This can be seen most clearly upon inspection of the specularly reflected spot along either azimuth. The diffuseness seen in the 5 ML coverage patterns can be attributed to the roughening of the surface as well as the insertion of dislocations and defects that accompany the onset of relaxation in the oxide

structure. The implications of maintaining a coherent interface are described in more detail in Chapter 7.

1. F. J. Walker and R. A. McKee, unpublished.

2. One ML is defined as the concentration of atoms on the (001) surface of silicon, i.e., 6.78×10^{14} atoms/cm^2.

3. R. A. McKee, F. J. Walker, and M. F. Chisholm, Phys. Rev. Lett. **81**, 3014 (1998).

4. R. Droopad, Z. Yu, J. Ramdani, L. Hilt, J. Curless, C. Overgaard, J. L. Edwards, J. Finder, K. Eisenbeiser, J. Wang, V. Kaushik, B-Y Ngyuen, and B. Ooms, J. Cryst. Growth. **227-228**, 936 (2001).

5. X-ray photoelectron spectroscopy (XPS) would potentially provide the most useful data to answer this question. Given the fact that the "silicide" layer is submonolayer and provides a minimal signal compared to the silicon substrate and the near overlap of the $2p$ binding energy that exists in the peaks in an XPS spectrum for silicon (~ 98.8-99.5 eV) and a silicide (~99.5-99.8 eV) [Ref. 6], conclusive determination remains elusive.

6. J. F. Moulder, W. F. Stickle, P. E. Sobol, and K. E. Bomben, *Handbook of X-ray Photoelectron Spectroscopy*, (Perkin Elmer Corporation, Minnesota, 1992).

7. Y. Liang, S. Gan, and M. Engelhard, Appl. Phys. Lett. **79**, 3591 (2001).

8. A. Herrera-Gomez, F. S. Aguirre-Tostado, Y. Sun, P.Pianetta, Z. Yu, D. Marshall, R. Droopad, and W. E. Spicer, J. Appl. Phys. **90**, 6070 (2001).

9. J. Wang, personal communication.

10. V. G. Lifshits, A. A. Saranin, A. V. Zotov, *Surface Phases on Silicon: Preparation, Structures, and Properties*, 1st ed. (Wiley, New York, 1994).

11. W. A. Henle, M. G. Ramsey, F. P. Netzer, and S. Witzel, Surf. Sci. **243**, 141 (1991).

12. W. C. Fan, N. J. Wu, and A. Ignatiev, Phys. Rev. B **42**, 1254 (1990).

13. A. Mesarwi, W. C. Fan, and A. Ignatiev, J. Appl. Phys. **68**, 3609 (1990).

14. W. C. Fan and A. Ignatiev, Phys. Rev. B **44**, 3110 (1991).

15. M. H. Yang and C. P. Flynn, Phys. Rev Lett. **62**, 2476 (1989).

16. S. Yadavalli, M. H. Yang, and C. P. Flynn, Phys. Rev. B **41**, 7961 (1990).

17. K. T. Jacob, and V. Varghese, J. Mater. Chem. **5**, 1059 (1995).

18. E. S. Hellman and E. H. Hartford, Jr., Appl. Phys. Lett. **64**, 1341 (1994).

19. T. Waho, S. Ogawa, and S. Maruyama, Jpn. J. Appl. Phys. **16**, 1875 (1977).

20. A. Fischer, Z. Feng, E. Bykov, G. Contreras-Puente, A. Compaan, F. de Landa Castillo-Alvarado, J. Avendano, and A. Mason, Appl. Phys. Lett. **70**, 3239 (1997).

21. H. Holzschuh and H. Suhr, Appl. Phys. Lett. **59**, 470 (1991).

22. H. Schlotterer, Solid-State Electron. **11**, 947 (1968).

23. A. C. Ipri and J. N. Zemel, J. Appl. Phys. **44**, 744 (1973).

24. P. R. Berger, K. Chang, P. Bhattacharya, J. Singh and K. K. Bajaj, Appl Phys. Lett. **53**, 684 (1988).